



Acoustic and electroacoustic spectroscopy for characterizing concentrated dispersions and emulsions

Andrei S. Dukhin*, Philip J. Goetz

Dispersion Technology Inc., 3 Hillside Avenue, Mt Kisco, NY 10549, USA

Abstract

We describe two different techniques (acoustics and electroacoustics), both of which employ ultrasound instead of light for extracting information about the properties of liquid-based dispersions. Ultrasound can propagate through samples that are not transparent for light, which open up many new applications not possible with classical light scattering methods. Acoustic and electroacoustic techniques offer a unique opportunity to characterize concentrated dispersion, emulsions and microemulsions in their natural states. Elimination of a dilution step required for most other techniques (light scattering, sedimentation, electrophoresis) is crucial for an adequate characterization of liquid dispersions, especially when the high concentration leads to structured systems. As with any macroscopic method, ultrasonic techniques characterize the sample in two steps. The first step is to measure some macroscopic property. The second step involves some theoretical treatment of the measured raw data which yields the desired information. Acoustic spectroscopy deals with measuring the attenuation of ultrasound within a certain frequency range. Electroacoustic spectroscopy has two implementations depending on the driving force. We emphasize here on the so-called Colloid Vibration Current (CVI) which is generated by the sound wave as it passes through the dispersion. A review of the theoretical basis of acoustics and electroacoustics is given, with emphasis on models that have been applied to concentrated systems. Recently, new theories have been developed for both acoustics and electroacoustics using a 'coupled phase model' and 'cell model concept'. The coupled phase model is widely used for describing a relative motion of the particles and liquid in the sound wave. The cell model

* Corresponding author. Tel.: +1-914-241-4777; fax: +1-914-241-4842.
E-mail address: dispensi@dispension.com (A.S. Dukhin).

approach opens the way to include both particle–particle interactions and polydispersity into the theoretical model. Experimental evidence is presented that shows that this new approach is successful in concentrated systems up to 45% vol. A short review of the possible applications of acoustics and electroacoustics measurements to a range of systems is presented including: ceramics, mixed dispersed systems, chemical–mechanical polishing abrasives, emulsions, microemulsions and latex materials. © 2001 Elsevier Science B.V. All rights reserved.

Keywords: Concentrated dispersions; Particle size; Zeta potential; Acoustics; Electroacoustics

Contents

1. Introduction	74
2. Coupled phase model	79
3. Cell model concept.	83
4. Hydrodynamic cell model.	84
5. Electrokinetic cell model	85
6. Theory of acoustics	87
7. Theory of electroacoustics	91
8. Special functions	96
9. Bubbles problem	97
10. Experimental test.	97
11. Acoustic attenuation measurement	98
12. Electroacoustic CVI measurement	99
13. Materials and experimental protocol	102
14. Results and discussion	104
15. Applications	109
16. Ceramics and other solid particles in liquids.	109
17. Emulsions, microemulsions and latex	119
18. Conclusions	127
Nomenclature	127
References	129

1. Introduction

There are two ultrasound-based techniques which are suitable for characterizing heterogeneous solid-in-liquid or liquid-in-liquid colloidal systems. The first is referred to as ‘acoustics’. It is somewhat simpler than the second, which is referred to as ‘electroacoustics’. Acoustics deals only with the acoustics properties of the dispersion such as the ‘attenuation’ and ‘sound speed’. Electroacoustics is more complicated because it is related to the coupling between the acoustic and electric properties of the dispersion.

The history of the acoustics can be traced back to the creation of the first hardware for measuring the acoustic properties of liquids more than 50 years ago at MIT [1] by Pellam and Galt. The first attempt to develop an acoustic theory for heterogeneous systems was by Sewell 90 years ago [2], whereas the general acoustic principles for dilute systems were successfully formulated 45 years ago by Epstein and Carhart [3]. A long list of applications and experiments using acoustic spectroscopy appears in several reviews [4,5]. Despite all these developments, acoustic spectroscopy is rarely mentioned in modern handbooks of colloid science [6,7].

Acoustics can provide reliable particle size information for concentrated dispersions without any dilution. There are examples for which acoustics yields size information at volume fractions above 40%. Such in-situ characterization of concentrated systems makes the acoustic method very useful and quite unique compared to alternative methods including light scattering where extreme dilution is usually required. Acoustics is also able to deal with low dispersed phase volume fractions and some systems can be characterized at less than 0.1% vol. This flexibility in concentration range provides an important overlap with classical methods.

Acoustics does not require calibration with a known colloid. It is calibrated on first principles and provides an absolute particle size distribution (within the constraints of the model). It is a big advantage over the modern back-light scattering technique which is also supposed to work in moderately concentrated dispersions [8]. In addition, the acoustics theory takes into account particle interaction [9] whereas the back-light scattering technique is lacking such a theory.

Acoustics is more suitable than light scattering methods for characterizing polydisperse systems. Acoustics yields particle size on a weight basis which makes it similar to sedimentation techniques. Light scattering methods are much more sensitive to the presence of larger particles because this phenomenon exhibits a stronger dependence on the particle size, such as fifth or sixth power. As a result light scattering methods tend to overestimate the amount of larger particles and are often not able to resolve the presence of small particles in very polydisperse systems.

In addition to particle size, acoustics can also provide information about the microstructure of dispersed systems. The acoustic spectrometer can be considered as a micro-rheometer. Unlike traditional rheometers, an acoustic spectrometer applies stresses over a very short distance, on the scale of microns, thus sensing the microstructure of the dispersed system. This feature of acoustics is only beginning to be exploited.

The operating principles of the acoustic spectrometer are quite simple. The acoustic spectrometer generates sound pulses that after passing through a sample are measured by a receiver. The passage through the sample system causes the sound energy to change in intensity and phase. The acoustic instrument measures the sound energy losses (attenuation) and the sound speed. The sound attenuates due to the interaction with the particles and liquid in the sample system. Acoustic spectrometers work generally in the frequency range of 1–100 MHz. This is a much higher sound frequency than the upper limit of our hearing which is approximately

0.02 MHz. The acoustic spectrometer is non-destructive and energy of the ultrasound is very low in contrast with traditional sonicators built for eliminating aggregation.

While the operating principles are relatively simple, the analysis of the attenuation data to obtain particle size distributions does involve a degree of complexity, since the experimental results must be fitted to rather complex theoretical models based on various acoustic loss mechanisms. The advent of high speed computers and the refinement of these theoretical models have made the inherent complexity of this analysis of little consequence. In comparison, many other particle sizing techniques such as photon correlation spectroscopy also rely on similar levels of complexity in analyzing the experimental results.

Acoustic methods are very robust and precise [10]. They are much less sensitive to contamination compared to the traditional light-based techniques because the high concentration of particles in the fresh sample dominates any small residue from the previous sample. It is a relatively fast technique as well. Normally one particle size measurement can be done in a few minutes. These features make acoustics very attractive for on-line particle size monitoring.

Electroacoustics is a relatively new technique compared to acoustics. The first reference to an electroacoustic effect was made by Debye [11] and there are several short historical reviews [12,13]. Electroacoustics is more complex than acoustics because an additional electric field is involved. Electroacoustics, in principle, can provide particle size information as well as zeta potential. There are two different implementations of electroacoustics, depending on which field is used as the driving force. Electrokinetic Sonic Amplitude (ESA) involves the generation of sound energy caused by the driving force of an applied electric field. Colloid Vibration Current (CVI) is the phenomenon where sound energy is applied to a system and a resultant electric field or current is created by the vibration of the colloid electric double layers.

There are two different opinions about the application of ultrasound-based techniques to characterizing colloidal dispersions discussed in the paper [14]. We believe that acoustics is much more powerful than electroacoustics for particle size characterization. At the same time electroacoustics is the wonderful tool for ζ -potential characterization. We gave several positive arguments supporting our viewpoint years ago in the paper [14]. Here we repeat them with some additions resulting from our long time experience.

Taking into account these arguments we suggested the combination of acoustics and electroacoustics. According to this scheme, acoustics provides the particle size distribution whereas electroacoustics is used only for ζ -potential characterization Table 1. We would like to stress here that electroacoustics has many advantages over traditional microelectrophoretic methods of ζ -potential measurement. These advantages are summarized in Table 2.

An instrument which offers the combined features of both acoustic and electroacoustic spectroscopy is very suitable and attractive for many applications. Table 3 gives a list of existing applications for this new characterization technique.

Table 1
Advantages of the acoustics over the electroacoustics for particle sizing

-
1. No calibration using colloid with the known particle size
 2. Much wider particle size range from 10 nm to 100 μm , comparing to the typical electroacoustic range from 100 nm to 10 μm .
 3. Particle size is independent of the assumptions and any influence of the particle double layers
 4. Particle sizing of uncharged particles
 5. Particle size at high conductivity
 6. Much less sensitive to the temperature variation
 7. Much less sensitive to contamination
-

Table 2
Advantages of the electroacoustics over microelectrophoresis for ζ -potential characterization

-
1. No dilution, volume fraction up to 50%
 2. Less sensitive to contamination
 3. Higher precision (± 0.1 mV)
 4. Low surface charges (down to 0.1 mV)
 5. Electrosmotic flow is not important
 6. Convection is not important
 7. Accurate for non-aqueous dispersions
-

This review describes the present state of both acoustics and electroacoustics. We give here a short overview of the modern theory using the same basic notions and principles for both acoustics and electroacoustics. Then, we describe experimental tests that have been performed in order to verify this theory. At the end we give some examples that illustrate the usefulness of these ultrasound-based techniques for characterizing real dispersions.

The interaction of ultrasound with a heterogeneous dispersed system involves various thermodynamic, hydrodynamic and electrodynamic effects. The general theoretical picture is rather complex, however, there is always an opportunity to apply some simplification in the case of the particular real dispersion. This fortunate feature of acoustics historically has been implemented in terms of

Table 3
List of existing applications for acoustic and electroacoustic spectroscopy

Aggregative stability	Food products
Cement slurries	Latex
Ceramics	Microemulsions
Chemical-mechanical polishing	Mixed disperse systems
Coal slurries	Nanosize particles
Coatings	Non-aqueous systems
Cosmetics	Paints
Environment protection	Photo materials
Flotation, ore enrichment	

various mechanisms of the ultrasound interactions with a dispersed system. Altogether six mechanisms are known: (1) viscous; (2) thermal; (3) scattering; (4) intrinsic; (5) structural; and (6) electrokinetic.

1. The 'viscous' mechanism is hydrodynamic in nature. It is related to the shear waves generated by the particle oscillating in the acoustic pressure field. These shear waves appear because of the difference in the densities of the particles and medium. The density contrast causes the particle motion with respect to the medium. As a result, the liquid layers in the particle vicinity slide relative to each other. The sliding non-stationary motion of the liquid near the particle is referred to as the 'shear wave'. This mechanism is important for acoustics. It causes losses of the acoustic energy due to the shear friction. Viscous dissipative losses are dominant for small rigid particles with sizes below $3\ \mu\text{m}$, such as oxides, pigments, paints, ceramics, cement, and graphite. The viscous mechanism is closely related to the electrokinetic mechanism which is also associated with the shear waves.
2. The 'thermal' mechanism is thermodynamic in nature and it is related to the temperature gradients generated near the particle surface. Temperature gradients are due to the thermodynamic coupling between pressure and temperature. This mechanism is also important for acoustics. Dissipation of the acoustic energy caused by thermal losses is the dominant attenuation effect for soft particles, including emulsion droplets and latex beads. For yet unknown reasons this thermodynamic effect does not show up in electroacoustics. There is a hypothesis [13] that it might be explained by different symmetry of thermodynamic and electrodynamic fields which eliminates their coupling.
4. The 'scattering' mechanism is essentially the same as in the case of the light scattering. Acoustic scattering does not produce dissipation of acoustic energy. Particles simply redirect a part of the acoustic energy flow and as a result this portion of the sound does not reach the sound transducer. The scattering mechanism contributes to the overall attenuation and is important for acoustics. This contribution is significant for larger particles ($> 3\ \mu\text{m}$) and high frequency ($> 10\ \text{MHz}$).
5. The 'intrinsic' mechanism is the part of acoustics. It causes losses of the acoustic energy due to the interaction of the sound wave with the materials of the particles and medium as homogeneous phases on a molecular level. It must be taken into account when overall attenuation is low which might have happened for the small particles or low volume fractions.
6. The 'structural' mechanism bridges acoustics with rheology. Actually one can consider the acoustic spectrometer as a microrheometer. In both cases we apply stress and measure respond. The difference is a scale of the applied stress. In the case of acoustics we apply stress over a half wavelength which is only approximately tenths of microns on the megahertz scale. The structural mechanism might contribute to the acoustic attenuation. Unfortunately, this mechanism is still not well described.
7. The 'electrokinetic' mechanism describes interaction of the ultrasound with the

double layer of particles. Oscillation of charged particles in the acoustic field leads to the generation of an alternating electrical field, and consequently to alternating electric current. This mechanism is a basis for electroacoustics. It turned out that its contribution to the acoustic attenuation is negligible. It is a very important feature of acoustics because it makes it independent on the electric properties of the dispersion including properties of the double layers.

There is no theory which would take into account all seven mechanisms. Derivation of such a theory is complicated by possible coupling between various mechanisms. Particle–particle interaction brings an additional factor which must be considered in the concentrated systems. Fortunately, there is an opportunity to simplify this theory dramatically by applying a so-called ‘long wave requirement’ [15] which requires the wave length of the sound wave λ to be larger than particle radius a .

$$\lambda \gg a \quad (1)$$

The ‘long wave requirement’ [Eq. (1)] restricts particle size for a given set of frequencies. Our experience shows that particle size must be below several tenths of microns for the frequency range from 1 to 100 MHz. This restriction is helpful for characterizing small particles.

Long wave requirement allows us to consider all mechanisms separately. For instance, we can express the total attenuation measured with the acoustic spectrometer α as a the sum of these four partial attenuations:

$$\alpha = \alpha_{\text{vis}} + \alpha_{\text{th}} + \alpha_{\text{sc}} + \alpha_{\text{int}} \quad (2)$$

where α_{vis} is the contribution of the viscous mechanism, α_{th} is the contribution of the thermal mechanism, α_{sc} is the contribution of the scattering mechanism and α_{int} is the attenuation in the pure liquid.

There is another approach to acoustics that employs a ‘short wave requirement’. It was introduced by Riebel [16]. This approach works only for large particles above 10 μm and requires limited input data about the sample.

Adopting the long wave requirement allows us to use a ‘coupled phase model’ [9,17,18] for describing relative motion of the particles and liquid and ‘cell model concept’ [19,20,25,26] for incorporating hydrodynamic and electrodynamic particle interaction. These two useful theoretical methods are described below.

This review describes the present state of both acoustics and electroacoustics. We give here a short overview of the modern theory using the same basic notions and principles for both acoustics and electroacoustics. Then, we describe experimental tests that have been performed in order to verify this theory. At the end we give some examples that illustrate the usefulness of these ultrasound-based techniques for characterizing real dispersions.

2. Coupled phase model

Let us consider the infinite small volume element in the dispersed system. There

is a differential force acting on this element, proportional to the pressure gradient of the sound wave ∇P . This external force is applied to both the particles and liquid and is distributed between particles and liquid according to the volume fraction φ .

Both particles and liquid move with an acceleration created by the sound wave pressure gradient. In addition, because of inertia effects, the particles move relative to the liquid which causes viscous friction forces acting between the particles and liquid.

The balance of these forces can be presented using the following system of equations written separately for particles and liquid:

$$-\varphi \nabla P = \varphi \rho_p \frac{\partial u_p}{\partial t} + \gamma(u_p - u_m) \quad (3)$$

$$-(1 - \varphi)\nabla P = (1 - \varphi)\rho_m \frac{\partial u_m}{\partial t} - \gamma(u_p - u_m) \quad (4)$$

where u_m , and u_p are velocities of the medium and particles in the laboratory frame of references, t is time and γ is a friction coefficient which is proportional to the volume fraction and particle hydrodynamic drag coefficient Ω

$$\gamma = \frac{9\eta\varphi\Omega}{2a^2}$$

$$F_f = 6\pi\eta a\Omega(u_p - u_m)$$

where η is dynamic viscosity, and a is the particle radius.

In addition, we can use the mass conservation law which might be presented as follows:

$$-\frac{\partial P}{\partial t} = M^*(1 - \varphi)\nabla u_m + M^*\varphi\nabla u_p \quad (5)$$

where M^* is a stress modulus (the reciprocal of compressibility) of the dispersed system, and t is a time.

The system of Eqs. (3)–(5) is well known in the field of acoustics. It has been used in several papers [9,17,18] for calculating sound speed and acoustic attenuation. It is valid without any restriction on volume fraction. Importantly, it is known that this system of equations yields a correct transition to the dilute case.

This system of equations is normally referred to as the ‘coupled phase model’. The word ‘model’ usually suggests the existence of some alternative formulation, but it is hard to imagine what one can change in this set of force balance equations, which essentially express Newton’s second law. Perhaps, the word ‘model’ is too pessimistic in this case.

The ‘coupled phase model’ opens an opportunity to describe a polydisperse system without using the superposition assumption. In order to do this we have to reformulate equations of the force balance for the polydisperse system.

The new system of N equations is:

$$\left(\frac{\rho_p}{\rho_m} - 1\right)\nabla P = \left(j\omega\rho_p + \frac{\gamma_i}{\varphi_i}\right)x_i + \frac{\rho_p}{(1-\varphi)\rho_m} \sum_i \gamma_i x_i \quad (9)$$

This system can be solved using the principle of mathematical induction. We guess solution for N fractions and then prove that the same solution works for $N + 1$ fraction. As a result we obtain the following expression for velocity of the i -th fraction particle relative to the liquid:

$$u_i - u_m = \frac{\left(\frac{\rho_p}{\rho_m} - 1\right)\nabla P}{\left(j\omega\rho_p + \frac{\gamma_i}{\varphi_i}\right) \left(1 + \frac{\rho_p}{(1-\varphi)\rho_m} \sum_{i=1}^N \frac{\gamma_i}{j\omega\rho_p + \frac{\gamma_i}{\varphi_i}}\right)} \quad (10)$$

This particle velocity is important for the further calculation in the electroacoustic theory. At the same time the ‘coupled phase model’ yields an important result for the acoustic theory. The system of Eqs. (6) and (7) combined with the mass conservation law allows us to calculate the complex wavenumber without using superposition assumption. This was done in the paper [9]. We reproduce the result here:

$$\frac{l^2 M^*}{\omega^2} = \frac{(1-\varphi)\rho_m + \sum_{i=1}^N \frac{\gamma_i(\text{Den}_i - j\omega\gamma_i)}{j\omega\text{Den}_i}}{\left(1-\varphi + \sum_{i=1}^N \frac{j\omega\varphi_i\gamma_i}{\text{Den}_i}\right)^2 - \sum_{i=1}^N \frac{\omega^2\varphi_i^2}{\text{Den}_i} \left(\rho_m - \varphi\rho_m + \sum_{i=1}^N \frac{\gamma_i(\text{Den}_i - j\omega\gamma_i)}{j\omega\text{Den}_i}\right)} \quad (11)$$

where

$$\text{Den}_i = -\omega^2\varphi_i\rho_p + j\omega\gamma_i + j\omega\delta_i + \beta_i$$

Parameters β_i and δ_i are two first virial coefficients which characterize oscillation of the structure in the case when particles are bound. These parameters link this theory to the rheology. Unfortunately, this link has not been exploited yet and in the current programs which are used in the instruments these parameters are assumed to be zero.

Expression 11 specifies the complex wavenumber neglecting thermodynamic effects. There is a version of the coupled phase model which take into account thermodynamic effects as well [21]. It is important in the case of the flexible particles when the ‘thermal’ mechanism becomes significant.

The coupled phase model does not assume the absence of the particle–particle

interaction. Parameters β_i and δ_i reflect the specific particles interaction like polymer bonds whereas the hydrodynamic particle–particle interaction is incorporated into the drag coefficient γ . We can take into account this hydrodynamic effect calculating γ using the ‘cell model concept’ which is described in the following section.

3. Cell model concept

The main idea of the ‘cell model’ is that each particle in the concentrated system is considered separately inside of the spherical cell of liquid associated only with a given individual particle. The cell boundary conditions formulated on the outer boundary of the cell reflect the particle–particle interaction.

In the past, the cell model has been applied only to monodisperse systems. This restriction allows one to define the radius of the cell. Equating the solid volume fraction of the each cell to the volume fraction of the entire system yields the following expression for the cell radius, b

$$b = \frac{a}{\sqrt[3]{\varphi}} \quad (12)$$

In the case of a polydisperse system, the introduction of the cell is more complicated because the liquid can be distributed between fractions in an infinite number of ways. However, the condition of mass conservation is still necessary.

Each fraction can be characterized by particles radii a_i , cell radii b_i , thickness of the liquid shell in the spherical cell $l_i = b_i - a_i$ and volume fraction φ_i . The mass conservation law relates these parameters together as follows:

$$\sum_{i=1}^N \left(1 + \frac{l_i}{a_i}\right)^3 \varphi_i = 1 \quad (13)$$

This expression might be considered as an equation with N unknown parameters l_i . An additional assumption is still necessary to determine the cell properties for the polydisperse system. This additional assumption should define the relationship between particle radii and shell thickness for each fraction. We suggest the following simple relationship:

$$l_i = la_i^n \quad (14)$$

This assumption reduces the number of unknown parameters to only two which are related by the following expression:

$$\sum_{i=1}^N (1 + la_i^{n-1})^3 \varphi_i = 1 \quad (15)$$

The parameter n is referred to as a ‘shell factor’. Two specific values of the shell factor correspond to easily understood cases. A shell factor of 0 depicts the case in

which the thickness of the liquid layer is independent on the particle size. A shell factor of 1 corresponds to the normal ‘superposition assumption’ which gives the same relationship between particles and cell radiuses in the monodisperse case, i.e. each particle is surrounded by a liquid shell which provides each particle with the same volume concentration as the volume concentration of the overall system.

In general, the ‘shell factor’ might be considered an adjustable parameter because it adjusts the dissipation of energy within the cells. However, our experience using this cell model with acoustics for particle sizing [22] indicates that a shell factor equal to 1 is almost always suitable. We take this value of n for the further derivations.

The cell model concept can be applied for describing the hydrodynamic effects as well as electrokinetic effects. The following sections present the short review of both types of the cell models.

4. Hydrodynamic cell model

There are two most widely used hydrodynamic cell models called according to the names of their authors: the Happel cell model [23] and the Kuwabara cell model [24]. Both of them are formulated for incompressible liquid. The long wavelength requirement [Eq. (1)] allows us to use this traditional hydrodynamics in the non-stationary case of the ultrasound field. The system of the equations for liquid velocity u and hydrodynamic pressure P is as following:

$$\rho_m \frac{du}{dt} = \eta \operatorname{rot} \operatorname{rot} u + \operatorname{grad} P \quad (16)$$

$$\operatorname{div} u = 0 \quad (17)$$

Both models apply the same boundary conditions at the surface of the particle:

$$u_r(r = a) = u_p - u_m \quad (18)$$

$$u_\theta(r = a) = -(u_p - u_m) \quad (19)$$

The boundary conditions at the surface of the cell are different. For the Kuwabara cell model it is given by the following equations:

$$\operatorname{rot} u_{r=b} = 0 \quad (20)$$

$$u_r(r = b) = 0 \quad (21)$$

In the case of the Happel cell model they are:

$$\Pi_{r\theta}(r=b) = \frac{1}{r} \frac{\partial u_r}{\partial \theta} + r \frac{\partial \frac{u_\theta}{r}}{\partial r} = 0 \quad (22)$$

$$u_r(r=b) = 0 \quad (23)$$

The general solution for the velocity field contains three unknown constants C , C_1 and C_2

$$u_r(r) = C \left(1 - \frac{b^3}{r^3}\right) + 1.5 \int_r^b \left(1 - \frac{x^3}{r^3}\right) h(x) dx \quad (24)$$

$$u_\theta(r) = -C \left(1 + \frac{b^3}{2r^3}\right) - 1.5 \int_r^b \left(1 + \frac{x^3}{2r^3}\right) h(x) dx \quad (25)$$

$$h(x) = C_1 h_1(x) + C_2 h_2(x) \quad (26)$$

The drag coefficient can be expressed in the following general form for both the Kuvabara and Happel cell models:

$$\Omega = -\frac{\alpha^2}{3} \left(\frac{d(C_1 h_1 + C_2 h_2)}{dx} + \frac{C_1 h_1 + C_2 h_2}{\alpha} \right)_{x=\alpha} - \frac{4j\alpha^2}{9} \quad (27)$$

where x is normalized the same way as α , coefficients C_1 and C_2 are different for two cell models:

	Kuvabara	Happel
C_1	$\frac{h_2(b)}{I}$	$\frac{bh_2(b) - 2I_{23}}{bI + 2(I_2 I_{13} - I_1 I_{23})}$
C_2	$\left[-\frac{h_1(b)}{I} \right]$	$-\frac{bh_1(b) - 2I_{13}}{bI + 2(I_2 I_{13} - I_1 I_{23})}$

The Happel cell model is more suited for acoustics because it describes more adequately energy dissipation, whereas the Kuvabara cell model is better for electroacoustics because it automatically yields the Onsager relationship [25,20].

5. Electrokinetic cell model

Electrokinetic cell models are the result of some generalization of the hydrodynamic cell models. There are many ways to perform this generalization and, correspondingly, many ways to create different electrokinetic cell models. The difference between electrokinetic cell models is related to the description of the

electric characteristics. The relationship between macroscopic experimentally measured electric properties and local electric properties calculated using cell concept varies for different cell models. For instance, the Levine–Neale cell model [27] specifies this relationship using one of the many possible analogies between local and macroscopic properties. Macroscopic properties are current density $\langle I \rangle$ and electric field strength $\langle E \rangle$. They are related with local electric current density I and the electric field $\nabla\phi$ according to the Levine–Neale cell model with the following expressions:

$$\langle I \rangle = \frac{I_r}{b \cos\theta}_{r=b} \quad (28)$$

$$\langle E \rangle = \frac{1}{\cos\theta} \frac{\partial\phi}{\partial r}_{r=b} \quad (29)$$

Relationships (28–29) are not unique. There are many other ways to relate macroscopic and local fields. It means that we need a set of criteria to select a proper cell model. These criteria have been suggested in the electrokinetic cell model created by Shilov and Zharkikh [25,26]. Their two criteria determine a proper choice of the macroscopic ‘fields’ and ‘flows’.

The first criteria is a well-known Onsager relationship [6] which constrain values of the macroscopic particles velocity relative to the liquid $\langle V \rangle$, macroscopic pressure $\langle P \rangle$, electric current $\langle I \rangle$ and field $\langle E \rangle$:

$$\frac{\langle V \rangle}{\langle I \rangle}_{\langle \nabla P \rangle = 0} = \frac{\langle E \rangle}{\langle \nabla P \rangle}_{\langle I \rangle = 0} \quad (30)$$

This relationship requires a certain expression for entropy production Σ :

$$\Sigma = \frac{1}{T} (\langle I \rangle \langle E \rangle + \langle V \rangle \langle \nabla P \rangle) \quad (31)$$

Shilov and Zharkikh used this relationship between ‘fields’, ‘flows’ and entropy production in order to derive the cell model condition for macroscopic properties. It turned out that the expression for the macroscopic field strength is different compared with the Levine–Neale:

$$\langle E \rangle = \frac{\phi}{b \cos\theta}_{r=b} \quad (32)$$

whereas expression for the macroscopic current is the same in both models.

This cell model yields the correct transition to the Smoluchowski law. Smoluchowski’s law is a very important test for any electrokinetic theory because it is valid for any geometry and volume fraction. Failure to satisfy the Smoluchowski law test is a clear indication that the theory is not correct. Shilov and Zharkikh

wrote in their paper that their theory met Smoluchowski's law requirement. They even made a stronger conclusion that it was the Levine–Neale cell model which did not reduce to the Smoluchowski law. This opinion is discussed in the paper [20]. It was shown again that this difference comes from a misunderstanding of the Smoluchowski law in the case of concentrated systems. The version of Smoluchowski's law which is valid in concentrated systems confirms the Shilov–Zharkikh cell model.

6. Theory of acoustics

The most well known acoustic theory for heterogeneous systems was developed by Epstein and Carhart [3], Allegra and Hawley [28]. The theory takes into account the four most important mechanisms (viscous, thermal, scattering and intrinsic) and is termed the 'ECAH theory'. It describes the acoustic attenuation for a monodisperse system of spherical particles and is valid only for dilute systems. Extensions of the ECAH theory to include polydispersity have typically assumed a simple linear superposition of the attenuation for each size fraction. The term 'spherical' is used to denote that all calculations are performed assuming that each particle can be adequately represented as a sphere.

Most importantly, the term 'dilute' is used to indicate the assumption that there are no particle–particle interactions. This fundamental limitation normally restricts the application of the resultant theory to dispersions with a volume fraction of less than a few volume percent. However, there is some evidence that the ECAH theory, in some very specific situations, does nevertheless provide a correct interpretation of experimental data, even for volume fractions surprisingly as large as 30%.

An early demonstration of this ability of the ECAH theory was provided by Allegra and Hawley. They observed an almost perfect correlation between experiment and ECAH theory for the following dispersions: a 20% by volume toluene emulsion; a 10% by volume hexadecane emulsion; and a 10% by volume polystyrene latex. Experiments with emulsions by McClements [29,30] has provided similar results. The recent work by Holmes et al. [31,32] also shows good agreement between the ECAH theory and experiments even for 30% by volume polystyrene latex. An absence of particle–particle interaction was also observed with neoprene latex [33].

It is important to note that the unexpected validity of the dilute ECAH theory for moderately concentrated systems has only been demonstrated in systems where the 'thermal losses' were dominant, such as emulsions and latex systems.

The difference between the 'viscous depth' and the 'thermal depth' provides an answer to the observed differences between emulsions and solid particle dispersions. These parameters characterize the penetration of the shear wave and thermal wave correspondingly into the liquid. Particles oscillating in the sound wave generate these waves which dampen in the particle vicinity. The characteristic distance for the shear wave amplitude to decay is the 'viscous depth' δ_v . The

corresponding distance for the thermal wave is the ‘thermal depth’ δ_t . The following expressions give values for the parameters in dilute systems:

$$\delta_v = \sqrt{\frac{2\nu}{\omega}} \quad (33)$$

$$\delta_t = \sqrt{\frac{2\tau_m}{\omega\rho_m C_p^m}} \quad (34)$$

where ν is the kinematic viscosity, ω is the sound frequency, ρ_m is the density, τ_m is heat conductance, C_p^m is a heat capacity at constant pressure of liquid.

The relationship between δ_v and δ_t has been considered before. For instance, McClements plots ‘thermal depth’ and ‘viscous depth’ vs. frequency [29,30]. It is easy to show that the ‘viscous depth’ is 2.6 times more than the ‘thermal depth’ in aqueous dispersions. As a result, the particle viscous layers overlap at the lower volume fraction more than the particle thermal layers. Overlap of the boundary layers is the measure of the corresponding particle–particle interaction. There is no particle interaction when corresponding boundary layers are sufficiently separated.

Thus, an increase in the dispersed volume fraction for a given frequency first leads to the overlap of the viscous layers because they extend further into the liquid. Thermal layers overlap at higher volume fractions. Therefore, the particle hydrodynamic interaction becomes more important at the lower volume fractions than the particle thermodynamic interaction.

Overlap of the boundary layers affects a critical frequency at which attenuation expressed in dB/cm/MHz reaches a maximum. For systems where the viscous acoustic losses dominate, the maximum is shifted to higher frequencies at high concentrations, which will result in a lower attenuation value for a given frequency. Therefore, if the attenuation is considered at a single frequency the attenuation will at first increase with a higher dispersed phase. Once the concentration is high enough, the attenuation curve and maximum shift to higher frequencies and the attenuation at the considered single frequency decreases. This effect is illustrated with a calculated attenuation spectra on Fig. 1 and later it is proved with an equilibrium dilution test [13].

The 2.6 times difference between δ_v and δ_t leads to a large difference in the volume fractions corresponding to the beginning of the boundary layers overlap. It is interesting that this important feature of the ‘thermal losses’ works for almost all liquids [21,34]. Therefore, ‘thermal losses’ are much less sensitive to the particle–particle interaction than ‘viscous losses’ for almost all known liquids. It makes the ECAH theory valid in a much wider range of emulsion volume fractions than one would expect.

There is one fact that follows from the values of the liquid’s thermal properties that makes it convenient to use the ECAH theory. In general, the ECAH theory

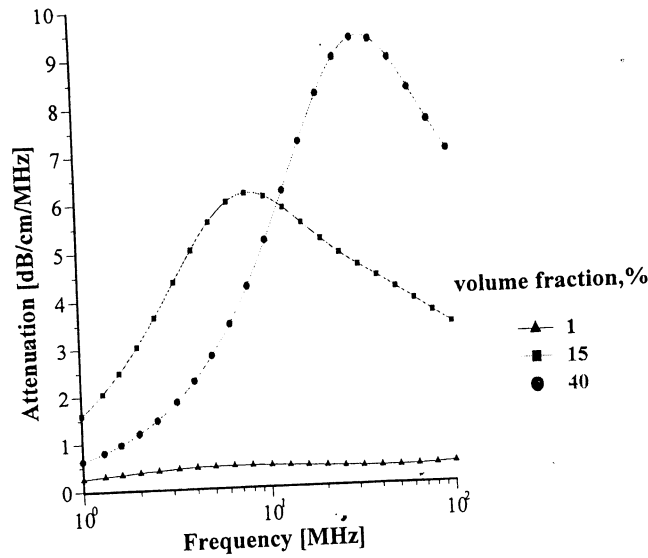


Fig. 1. Attenuation spectra calculated for various volume fractions of the dispersion of 1- μm particles.

requires information about three thermodynamic properties: thermal conductivity τ ; heat capacity C_p ; and thermal expansion β . It turns out that τ and C_p are almost the same for all liquids except water [35]. The number of required parameters is then reduced to one—thermal expansion. The parameter of the thermal expansion then plays the same role in ‘thermal losses’ as density in ‘viscous losses’.

The ECAH theory has a big disadvantage of being mathematically complex. It cannot be generalized for particle–particle interactions. Long wave requirement allows us to overcome this problem by simplifying the theory. We can express the total attenuation measured with the acoustic spectrometer as the sum of these four partial attenuations [Eq. (2)] if the long wave requirement is valid. In addition, by restricting frequency and particle size with the long wave requirement we can use the simpler explicit expression for the thermal losses α_{th} obtained initially by Isakovich [36] and confirmed later by Epstein and Carhart [3], Allegra and Hawley [28]:

$$\alpha_{th} = \frac{3\varphi T c_m \rho_m \tau_m}{2a^2} \left(\frac{\beta_m}{\rho_m C_p^m} - \frac{\beta_p}{\rho_p C_p^p} \right)^2 \text{Re} \left(\frac{1}{1 - jz_m} - \frac{\tau_m \tanh z_p}{\tau_p \tanh z_p - z_p} \right) \quad (35)$$

where

$$z = (1 + j)a \sqrt{\frac{\omega \rho C_p}{2\tau}}$$

At the same time the long wave requirement provides a sufficient simplification of the theory for taking into account the particle–particle hydrodynamic interaction into the theory of the viscous losses. It has been done in the work [9] on the basis of the ‘coupled phase model’ [17,18]. This new theory works up to 40% volume and yields the following expression for the complex wavenumber l assuming viscous losses as the only one mechanism of the particles interaction with the sound wave:

$$\frac{l^2 M^*}{\omega^2} = \frac{\rho_m(1-\varphi) + \rho_p \sum_{i=1}^N \frac{\varphi_i \gamma_i}{j\omega\rho_p\varphi_i + \gamma_i}}{(1-\varphi)^2 + \sum_{i=1}^N \frac{\varphi_i(\varphi-2)\gamma_i - \varphi_i^2(1-\varphi)\rho_m}{j\omega\rho_p\varphi_i - \gamma_i}} \quad (36)$$

where Ω is a drag coefficient specified above, M^* is the stress modulus which can be expressed in terms of densities and sound speeds as follows:

$$M^* = \frac{\rho_p \rho_m c_p^2 c_m^2}{\varphi \rho_m c_m^2 + (1-\varphi)\rho_p c_p^2}$$

Expression (36) specifies the value of viscous losses:

$$\alpha_{\text{vis}} = -\text{Im}l \quad (37)$$

This theory can be used also for calculating sound speed of the dispersions where viscous losses are dominant.

$$c_s = \frac{\omega}{\text{Re}l} \quad (38)$$

Expressions for calculating intrinsic α_{int} and scattering losses α_{sc} for long wave limit are given in the papers of McClements [4,29,30]. He uses the term ‘lossless scatterers’ for describing sound propagation through the system when dissipative mechanisms of viscous and thermal losses are negligible. Intrinsic attenuation in such a system can be expressed as the following [33]:

$$\alpha_{\text{int}} = \frac{(1-\varphi)\frac{\alpha_m}{c_m} + \varphi\frac{\rho_m\alpha_p}{\rho_p\alpha_m}}{\sqrt{\frac{1-\varphi}{c_m^2} + \frac{\varphi\rho_m}{\rho_p c_p^2}}} \sqrt{\frac{\rho_s}{\rho_m}} \quad (39)$$

where α_m and α_p are attenuations of the medium and particle materials.

Scattering attenuation can be calculated following the Waterman–Truell theory [37] which yields the following expression for the complex wavenumber l_s associated with scattering:

$$\frac{l_s^2}{l_m^2} = \left(1 - \frac{3j\varphi}{(l_m a)^3} A_0\right) \left(1 - \frac{9j\varphi}{(l_m a)^3} A_1\right) \quad (40)$$

where A_0 and A_1 are monopole and dipole scattering coefficients calculated for a single particle,

$$l_s = \frac{\omega}{c_s} + j\alpha_{sc}$$

$$l_m = \frac{\omega}{c_m} + j\alpha_m$$

The simplest formula expressing the scattering losses in terms of densities and sound speeds can be derived from Eq. (10) for a single scattering:

$$\alpha_{sc} = \frac{\varphi\omega^4 a^3}{2c_m^4} \left[\frac{1}{3} \left(1 - \frac{\rho_m c_m^2}{\rho_p c_p^2}\right)^2 + \left(\frac{\rho_p - \rho_m}{2\rho_p + \rho_m}\right)^2 \right] \quad (41)$$

It is seen that scattering losses depend on frequency very strongly. According to our experience scattering is important only for large particle ($> 3 \mu\text{m}$) and at high frequencies ($> 10 \text{ MHz}$).

There are two recent developments in the theory of acoustics that deserve to be mentioned here. The first one is a theory of acoustics for flocculated emulsions [38]. It is based on the ECAH theory but it uses in addition an ‘effective medium’ approach for calculating thermal properties of the flocs. The success of this idea is related to the feature of the thermal losses that allows for insignificant particle–particle interactions even at high volume fractions. This mechanism of acoustic energy dissipation does not require relative motion of the particle and liquid. Spherical symmetrical oscillation is the major term in these kinds of losses. This provides the opportunity to replace the floc with an imaginary particle assuming a proper choice for the thermal expansion.

Another significant recent development is due to Samuel Temkin. He offers in his recent papers [39,40] a new approach to the acoustic theory. Instead of assuming a model dispersion consisting of spherical particles in a Newtonian liquid, he suggests that the thermodynamic approach is explored as far as possible. This new theory is based on particle velocities and temperature fluctuations. Tempkin’s theory yields some unusual results, but has not yet been used in commercially available instruments.

7. Theory of electroacoustics

Whereas acoustic spectroscopy describes the combined effect of all loss mechanisms, electroacoustic spectroscopy, as it is presently formulated, emphasizes only the electrokinetic mechanism.

In acoustic spectroscopy sound is utilized as both the excitation and the measured variable, and therefore, there is but one basic implementation. In contrast, electroacoustic spectroscopy deals with the interaction of electric and acoustic fields and therefore, there are two possible implementations. One can apply a sound field and measure the resultant electric current which is referred to as the colloid vibration current (CVI), or conversely one can apply an electric field and measure the resultant acoustic field which is referred to as the electroacoustic amplitude (ESA).

CVP occurs when the density of the particles ρ_p differs from that of the medium ρ_m , and the particles move relative to the medium under the influence of an acoustic wave. This motion causes a displacement of the internal and external parts of the double layer (DL) and is usually referred to as a polarization of the DL [44]. The displacement of opposite charges gives rise to a dipole moment and the superposition of the electric fields of these induced dipole moments over the collection of particles gives rise to a macroscopic electric current defined as the Colloid Vibration Current (CVI). Thus, the fourth mechanism of particle interaction with sound leads to the transformation of part of the acoustic energy to electric energy. This electric energy may then be dissipated if the opportunity for electric current flow exists.

ESA occurs when an alternating electric field is applied to the disperse system [12]. If the zeta potential of the particle is greater than zero, then the oscillating electrophoretic motion of the charged dispersed particles generates a sound wave. Both electroacoustic parameters CVI and ESA can be experimentally measured. The CVI or ESA spectrum is the experimental output from electroacoustic spectroscopy. Both of these spectra contain information about ζ -potential and PSD, however, only one of the electroacoustic spectra is required because both of them contain essentially the same information about the dispersed system.

The conversion of electroacoustic spectra into PSD requires a theoretical model of the electroacoustic phenomena. This conversion procedure is much more complicated for electroacoustics compared to acoustics because of the additional complications arising from the added electric field.

There are two quite different approaches to derive an electroacoustic theory. Historically the first began with works by Enderby and Booth [41,42]. They simply tried to solve a system of classical electrokinetic equations without using any thermodynamic relationships. It was very complex because they took into account surface conductivity effects. Although this initial theory was valid only for dilute systems, this approach was later expanded by Malrow et al. [43], who tried to generalize it for concentrated systems using a Levine cell model. Unfortunately, this first attempt to create an electroacoustic theory for concentrates was not successful because the Levine cell model is not suitable for this purpose [13].

An alternative approach to the electroacoustic theory was suggested later by O'Brien [45,46]. He introduced the concept of a dynamic electrophoretic mobility μ_d and suggested a relationship between this parameter and the measured electroacoustic parameters such as Colloid Vibration Current (CVI) or Electroacoustic Amplitude (ESA):

$$\text{ESA (CVI)} = C_{\text{cal}} \frac{\rho_p - \rho_m}{\rho_m} \varphi \mu_d E(\nabla P) \quad (42)$$

where C_{cal} is a cell constant, P is the hydrodynamic pressure, and E is the external electric field strength.

Later O'Brien stated that his relationship is valid for the concentrated system as well. This statement turned out not to be true [13].

According to O'Brien a complete functional dependence of ESA (CVI) on the key parameters like ζ -potential, particle size and frequency is incorporated into dynamic electrophoretic mobility. The coefficient of proportionality between ESA (CVI) and μ_d is frequency-independent as well as independent of particle size and ζ -potential. This peculiarity of Eq. (12) made dynamic electrophoretic mobility a central parameter of the electroacoustic theory.

The first theory of the dynamic electrophoretic mobility which relates this parameter with other properties of the dispersed system was created initially by O'Brien for the dilute case only, neglecting particle–particle interaction. We call this version the 'dilute O'Brien's theory'.

Later he applied the Levine cell model trying to expand the dynamic electrophoretic theory to concentrated systems [46]. This work was generalized recently by Ohshima [47]. We call this version the 'O'Brien–Levine' theory.

The last development of this approach was made recently by Ohshima et al. [20,48,49]. We used the Shilov–Zharkikh cell model for dynamic electrophoretic mobility. We call the combination of O'Brien's relationship and our dynamic electrophoretic mobility theory the 'hybrid O'Brien's theory'.

For a time, it looked like O'Brien's approach had won out over the other approach because it appeared to yield a desirable electroacoustic theory for the concentrated case. However, one important question remains unsolved. In principle these two approaches must give the same result. It is not clear if it is the case. These two approaches are completely independent and the relationship between them is not known even in the dilute case. It is obvious that such a comparison must be done. It would provide a strong support for O'Brien's theory if it confirms that two approaches merge. The first approach is somewhat more basic. It needs only major well tested electrokinetic equations.

The new theory based on the first approach has been created by Dukhin et al. [13,50] for the simpler case of the CVI and/or CVP when the gradient of pressure is a driving force generating the electroacoustic signal. We would like to be cautious concerning expanding this new theory to the ESA phenomenon. It turned out that the problem of frame of references has different implications for these different electroacoustic effects.

This new theory applies several assumptions. First, it is valid only for a thin double layer

$$\kappa a \gg 1 \quad (43)$$

where κ is the reciprocal Debye length.

Second, it assumes surface conductivity κ^s to be the same for all particles independent of their size.

Third, it considers frequency only below Maxwell–Wagner dispersion [51]:

$$\omega \ll \omega_e = \frac{K_m}{\varepsilon \varepsilon_0} \quad (44)$$

where ε and ε_0 are dielectric permittivities of the medium and vacuum, K_m is the conductivity of the medium.

This improved electroacoustic theory yields the following expression for CVI:

$$\text{CVI} = \frac{9\varepsilon\varepsilon_0\zeta(\rho_p - \rho_m)\nabla P}{4\eta} \times \frac{\sum_{i=1}^N \frac{1}{(Du_i + 1) - (Du_i - 0.5)\varphi} \frac{\varphi_i h(\alpha_i)}{j\alpha_i I(\alpha_i) \left(\rho_p - \rho_m \left(\frac{3H_i}{2I_i} + 1 \right) \right)}}{1 - \frac{\rho_p}{1 - \varphi} \sum_{i=1}^N \frac{\varphi_i \left(\frac{3H_i}{2I_i} + 1 \right)}{\rho_p - \rho_m \left(\frac{3H_i}{2I_i} + 1 \right)}} \quad (45)$$

where: $\alpha = a\sqrt{\omega}/2v$, $\beta = b\alpha/a$, special functions h , H and I are given below, $H_i = H(\alpha_i)$, $I_i = I(\alpha_i)$ and

$$Du_i = \frac{\kappa^\sigma}{K_m a_i} \quad (46)$$

This theory takes into account surface conductivity effects and as a result is valid for any value of the Dukhin number. This dimensionless parameter was introduced by Lyklema [6].

It turned out that there is a contradiction between the new electroacoustic theory and O'Brien's theory even modified with the new expression for dynamic mobility. Fig. 2 illustrates significance of the difference between two theories. Which one is correct?

There is an opportunity to answer this question using the quasi-stationary limit of low frequencies. It is possible to derive an independent expression for CVI in this stationary case using the Onsager relationship and Smoluchowski's law. Comparison of both theories with this low frequency limit shows that the new theory [Eq. (45)] satisfies the transition requirement to the stationary case whereas the O'Brien theory does not.

This conclusion was proved experimentally as it would be shown below. Failure of the O'Brien's relationship to satisfy the Onsager principle and experiment is very unfortunate for the electroacoustic theory because it prevents us

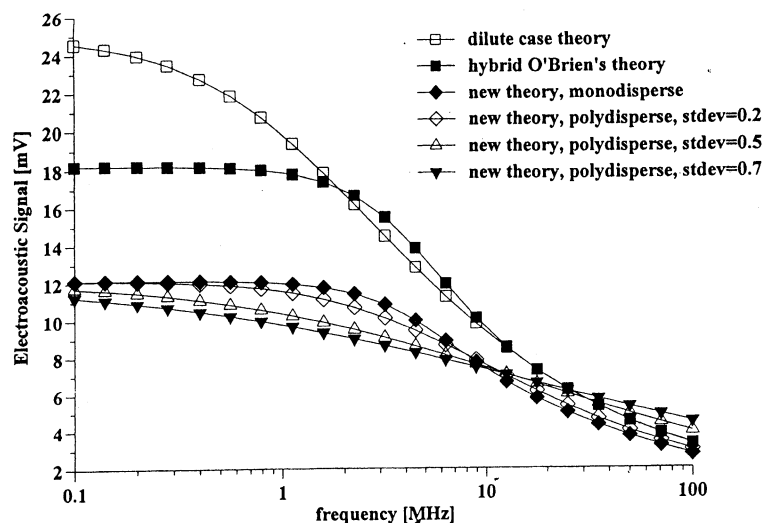


Fig. 2. Theoretically calculated normalized CVI [Eq. (22)] vs. frequency for dispersion with 20% vol. of 1- μm particles. Density of the liquid is 1 g/cu.cm, and of the particles, 2 g/cu.cm.

from using a very convenient Eq. (42) and the notion of dynamic electrophoretic mobility.

We would like to stress that according to our knowledge of the commercially available electroacoustic spectrometer based on the ESA principle-Acoustosizer of Colloidal Dynamics, applies empirical correction for calculating ζ -potential from the ESA signal. It follows directly from the recent review published by Hunter who is one of the Acoustosizer authors [12]. This correction is necessary because, as Hunter admits, their theory is valid only up to 5% vol. This empirical correction works and reduces dramatically error of the Acoustosizer in some concentrated systems. Unfortunately, this empirical correction mask results of theoretically justified calculations.

So far, the new electroacoustic theory has been tested with rigid heavy particles only. It is not clear yet how it will work for emulsions as there were no experimental data with emulsions available. This concern is related to the fact that this new theory as well as O'Brien's theory neglect thermodynamic effects. It is rather surprising as the thermodynamic effect of 'thermal losses' is dominant for acoustics of emulsions. It is not clear yet why electroacoustics is so different from acoustics for thermodynamic effects not to be important.

A simple hypothesis which might explain this difference is that electroacoustics is related to the displacement of the electric charges in the double layer (DL). This displacement is characterized by dipole symmetry ($E = f(r) \cos \theta$). At the same time 'thermal losses' measured by acoustics are associated mostly with spherical symmetry. They are caused by oscillation of the particle's volume in the sound

wave. It is clear that such a spherically symmetrical oscillation does not necessarily cause displacement of electric charges with dipole structure.

This is a hypothesis, and a fundamental theory that will take into account the thermodynamic effects in addition to electrodynamic and hydrodynamic effects should resolve this question. The electroacoustic theory of emulsions will not be complete unless such a theory is developed.

Nevertheless, electroacoustics even at its present stage can yield very important information about electric surface properties of emulsions as will be shown below.

8. Special functions

There are several special functions used in the above mentioned theory. They are specified below.

$$H(\alpha) = \frac{ih(\alpha)}{2\alpha} - \frac{idh(x)}{2dx} \Big|_{x=\alpha}$$

$$h(x) = h_1(x)h_2(\beta) - h_1(\beta)h_2(x)$$

$$I = I(\beta) - I(\alpha)$$

$$I(x) = -h_1(\beta)e^{x(1+j)} \left[\frac{3(1-x)}{2\beta^3} + j \left(\frac{x^2}{\beta^3} - \frac{3x}{2\beta^3} - \frac{1}{x} \right) \right] + h_2(\beta)e^{-x(1+j)} \\ \times \left[3 \frac{(1-x)}{2\beta^3} + j \left(\frac{x^2}{\beta^3} + \frac{3x}{2\beta^3} - \frac{1}{x} \right) \right]$$

$$I_1 = -j \frac{e^{-x(1+j)} \Big|_{x=a}^{x=b}}{x}$$

$$I_2 = -j \frac{e^{x(1+j)} \Big|_{x=a}^{x=b}}{x}$$

$$I_{13} = - \frac{e^{-x(1+j)} \Big|_{x=a}^{x=b}}{b^3} [1.5(x+1) + j(x^2 + 1.5x)]$$

$$I_{23} = \frac{e^{x(1+j)} \Big|_{x=a}^{x=b}}{b^3} [1.5(x-1) + j(-x^2 + 1.5x)]$$

$$h_1(x) = \frac{\exp(-x)}{x} \left[\frac{x+1}{x} \sin x - \cos x + j \left(\frac{x+1}{x} \cos x + \sin x \right) \right]$$

$$h_2(x) = \frac{\exp(x)}{x} \left[\frac{x-1}{x} \sin x + \cos x + j \left(\frac{1-x}{x} \cos x + \sin x \right) \right]$$

9. Bubbles problem

One of the experimental problems that can affect acoustics is the presence of air bubbles during measurements. While bubbles will affect sound attenuation and speed, it is worth considering how much of an effect they really have and whether the bubbles will detract from the acoustic techniques:

1. It has been determined that acoustic spectra are affected by bubbles. An acoustic theory describing sound propagation through bubbly liquid has been created by Foldy [52], and confirmed experimentally in 1940–1950 [53,54].
2. Contribution of bubbles to sound speed and attenuation depends on the bubble size and sound frequency. For instance, a 100- μm bubble has a resonance frequency of approximately 60 KHz. This frequency is reciprocally proportional to the bubble diameter. A bubble of 10 μm diameter will have a resonance frequency of approximately 0.6 MHz.
3. Acoustic spectroscopy of dispersed systems operates at frequencies above 1 MHz and usually up to 100 MHz. The size of the bubbles must be well below 10 μm in order to affect the complete frequency range of the acoustic spectrometer.
4. Bubbles of sizes below 10 μm are very unstable as is known from general colloid chemistry and the theory of flotation. 'Colloid-sized gas bubbles have astonishingly short lifetimes, normally between 1 μs and 1 ms' [55]. They simply dissolve in liquid because of their high curvature.

Bubbles can only affect the low frequency part of the acoustic spectra below 10 MHz. The frequency range from 10 to 100 MHz is available for particle characterization even in the bubbly liquids. The acoustic spectrometer can do both, sense bubbles and characterize particle size. This conclusion was confirmed with thousands of measurements performed with hundreds of different systems. Sensitivity to bubbles, in fact, is an important advantage of acoustics over electroacoustics. The presence of bubbles can affect the properties of the solid dispersed phase. For instance, bubbles can be centers of aggregation which might make them an important factor controlling stability.

10. Experimental test

The main goal of this experiment is testing validity of the acoustic and electro-

acoustic theory in concentrated systems. This test has been performed in the work [13]. Equilibrium dilution is the logical experimental protocol for achieving this goal because it provides a simple criterion of the theory. Equilibrium dilution maintains the same chemical composition of the dispersion medium for all volume fractions. As a result, parameters which are sensitive to the chemistry must be the same for all volume fractions. It means that the ζ -potential calculated from the CVI is supposed to remain the same for all volume fractions. Variation of the ζ -potential with volume fraction is the indication that the particular theory does not reflect volume fraction dependence properly.

The same test might be applied to the particle size distribution (PSD), however, with some degree of doubt. We cannot eliminate completely the possibility of aggregation induced by increasing volume fraction even at the same chemical composition. We can only be sure that particle size must not become smaller with increasing volume fraction.

We perform this dilution test with two different dispersions: silica Ludox and rutile R-746 produced by Dupont. We use two different techniques for producing the equilibrium dispersion medium for dilution: dialysis and centrifugation. We perform this experiment with the Acoustic and Electroacoustic Spectrometer DT-1200 [56,57]. This instrument spectrometer consists of two blocks: electronic block and sensor block. All electronics are placed on two special purpose boards (Signal Processor and Interface). It requires also a conventional Data Acquisition card. The Signal Processor board and DAC are placed inside of a personal computer which performs an interface with the user using Windows-95-based software.

The sensor block contains two sensors: an acoustic sensor for measuring attenuation and an electroacoustic sensor for measuring CVI. The next sections describe these sensors separately.

11. Acoustic attenuation measurement

The acoustic sensor has two piezo crystal transducers. The gap between the transmitter and receiver is variable in steps. In default it changes from 0.15 mm up to 20 mm in 21 steps. The transmitter generates acoustic pulses of certain frequency and length. The basic frequency of pulse changes in steps as well. In default it changes from 3 to 100 MHz in 18 steps. The number of pulses collected for each gap and each frequency is automatically adjustable in order to reach the target signal-to-noise ratio.

The acoustic sensor measures energy losses. There are several sources of these losses. Part of the pulse energy is lost in electronics. Another part of the energy is lost due to the limited efficiency of the piezo electric transducer to convert electric pulse to the sound pulse and visa versa. The most important part of the energy loss occurs while the ultrasound pulse propagates through the sample and interacts with dispersion. This last energy loss (colloid loss) is the target but actually acoustic sensor measures total energy losses including all possible sources. In order to

extract colloid losses from the total losses we should measure independently losses in electronics and losses in transducers. It is done automatically at the beginning of every measurement.

The acoustic sensor measures also sound speed at the one chosen frequency. It makes this using the time of pulse arrival to the receiver. The instrument automatically adjusts pulse sampling depending on the value of the sound speed. It is necessary for eliminating possible artifacts like excess attenuation at low frequencies.

The experimental output of the acoustic sensor is the attenuation frequency spectra in dB/cm/MHz. This experimental data is independent on any assumptions about sample which makes it very valuable.

In order to calculate particle size from the attenuation spectra one has to apply theory and corresponding theoretical assumptions.

12. Electroacoustic CVI measurement

The electroacoustic sensor has two parts: a piezoelectric transducer with a critical frequency of 10 MHz and an electroacoustic antenna. There is another design where a sensing electrode is placed on the surface of the transducer. We call this design the 'electroacoustic probe'.

The antenna is designed as two coaxial electrodes separated with a non-conducting rigid ceramic insert. Internal electric impedance between these electrodes can be selected depending on the conductivity range of the samples by means of an internal transformer. The transformer is selected such that the input impedance is significantly less than the external impedance of the sample such that the resultant signal is proportional to the short circuit current. This transformer is located just behind the central electrode in order to minimize the stray capacitance.

The transmitting transducer and the receiving antenna are mounted on the opposite walls of the sample chamber such that the gap between the faces is 5 mm.

The Signal Processor generates the transmit gate which defines the 1 W pulse generated in the Interface module as well as the necessary signals to set the frequency. Electroacoustic measurement can be performed either for one frequency or for the chosen set of frequencies from 1 to 100 MHz. The transducer converts these pulses to the sound pulses with some certain efficiency. The sound pulse propagates through the quartz delay rod and eventually through the sample. The acoustic pulse propagating through the sample excites particles, disturbs their double layers. Particles gain dipole moments because of this excitation. These dipole moments generate electric field. This electric field changes the electric potential of the central electrode of the electroacoustic antenna. Difference of the electric potentials between the central electrode and the external reference electrode causes an electric current. This current is registered as the Colloid Vibration Current.

The value of this current is very low. It takes averaging of at least 800 pulses in order to achieve the high signal-to-noise ratio. The number of pulses depends on

the acoustic properties of the colloid. The measurement of CVI in low conducting oil-based systems requires averaging of millions of pulses. In principle, this method makes it possible to measure any low energy signals.

We suggest to interpret this measurement as propagation of the pulse through the transmission line with certain energy losses at different points. This approach allows us to eliminate measurement of the absolute powers. We simply compare pulse intensity before and after transmission and take into account all internal energy losses. This idea is accomplished as described below.

At the beginning of each measurement the Interface routes the pulses to a reference attenuator channel consisting of a fixed 40 dB attenuator and similarly routes the output of this precision attenuator to the input section of the Signal processor. Since the precision attenuator has a known response over the entire frequency range, this step allows us to characterize all energy losses in the measuring circuits at each frequency.

The next step in the measurement is to determine the losses in the electroacoustic sensor. The Signal Processor now commands the Interface to substitute the electroacoustic sensor for the reference attenuator. The 1 W pulses are now sent to the transmitting transducer which converts these electric pulses to sound pulses. We have certain energy losses at this point. These losses depend on the transducer efficiency and are pretty much constant.

The sound pulses propagate through the quartz delay rod and eventually reaches the surface of the transducer which faces dispersion. It loses some energy at this point because of the reflection caused by mismatch of the acoustic impedances of the delay rod (Z_r) and dispersed system (Z_s).

Some part of the pulse passes into the gap between the transducers which is filled with the dispersion under test, and propagates through it. It loses energy during propagation due to the attenuation.

At last this sound pulse reaches electroacoustic antenna which converts it back to an electrical signal. This conversion is also related to energy losses.

This final electric pulse is routed through the interface to the input signal port on the Signal Processor where the signal level of the acoustic sensor output is measured. Comparison of the amplitude and phase of the electroacoustic sensor output pulse with that of the reference channel output pulse allows the program to calculate precisely the overall loss in the sensor at each frequency.

Experimental output of the electroacoustic sensor S_{exp} is ratio of the intensity of the input electric pulse to the transducer I_{in} to the output electric pulse in the antenna I_{out}

$$S_{\text{exp}} = \frac{I_{\text{out}}}{I_{\text{in}}} \quad (47)$$

The intensity of the input electric pulse is related to the intensity of the sound pulse in the delay rod through some constant C_{tr} which is a measure of the transducer efficiency and energy losses at this point:

$$I_{\text{rod}} = C_{\text{tr}} I_{\text{in}} \quad (48)$$

Intensity of the sound in the delay rod is proportional to a square of the sound pressure here P_{rod} :

$$P_{\text{rod}} = \sqrt{2\rho_{\text{rod}} c_{\text{rod}} C_{\text{tr}} I_{\text{in}}} \quad (49)$$

where ρ_{rod} and c_{rod} are density and sound speed of the rod material.

At the other end we can use the definition of the electric pulse intensity as a square of the electric current in the antenna which is CVI:

$$I_{\text{out}} = \text{CVI}^2 C_{\text{ant}} \quad (50)$$

where constant C_{ant} depends on geometrical factor of the CVI space distribution in the vicinity of the antenna and electric properties of the antenna only for the proper ration of the electric impedancies of the antenna and dispersed system.

Substituting Eq. (50) into Eq. (47) we obtain the following expression relating CVI with the measured parameter S_{exp} :

$$\frac{\text{CVI}}{P_{\text{rod}}} = \sqrt{S_{\text{exp}} / C_{\text{tr}} C_{\text{ant}} 2\rho_{\text{rod}} c_{\text{rod}}} \quad (51)$$

The value of CVI depends on the pressure near the antenna surface P_{ant} . This pressure is lower than the pressure in the rod P_{rod} because of the reflection losses on the rod surface and attenuation of the pulse in the dispersion. There are two ways to take into account these effects. We can either measure corresponding losses using reflected pulses or we can calculate these losses. If we choose the second way we should use the following corrections:

$$P_{\text{ant}} = P_{\text{rod}} \frac{2Z_s}{Z_s + Z_{\text{rod}}} \text{EXP}\left(-\frac{\alpha L}{2}\right) \quad (52)$$

where α is attenuation of the sound intensity expressed in Np/cm, L is the distance between the transducer and antenna in cm. These corrections lead to the following expression for CVI:

$$\frac{\text{CVI}}{P_{\text{ant}}} = \sqrt{S_{\text{exp}} / 2C_{\text{ant}} C_{\text{tr}} \rho_{\text{rod}} c_{\text{rod}}} \frac{Z_s + Z_{\text{rod}}}{2Z_s} \text{EXP}\left(\frac{\alpha L}{2}\right) \quad (53)$$

The gradient of pressure ∇P in Eq. (19) for CVI equals to the gradient of the pressure P_{ant} . Using this fact and substituting CVI from Eq. (53) we obtain the following equation relating properties of the dispersion with the measured parameter S_{exp} :

$$\frac{3\varepsilon \varepsilon_0 \zeta (1 - \varphi) \varphi (\rho_p - \rho_s)}{2\eta(1 + 0.5\varphi) \rho_s} G(a, \varphi) = \frac{cC_{\text{cal}}}{f} \left(1 - i \frac{\alpha c}{2\omega}\right) \sqrt{S_{\text{exp}}} \frac{Z_s + Z_{\text{rod}}}{2Z_s}$$

$$\times \text{EXP}\left(\frac{\alpha L}{2}\right) \quad (54)$$

where c is sound speed in the dispersion, f is frequency in Hz.

Eq. (54) contains an unknown calibration constant C_{cal} , which is independent of the properties of the dispersion. This constant can be calibrated out using calibration with the known colloid. We use for this purpose silica Ludox at 10% wt. diluted with KCl 10^{-2} mol/l. These silica particles have a ζ -potential of -38 mV at pH 9.3.

Expression (54) can be used for calculating either ζ -potential only in the case of a single frequency measurement or both ζ -potential and particle size in the case of multiple frequencies.

It is important to mention that there is a coupling between attenuation and CVI measurements according to Eq. (54). On the one hand, this coupling provides an additional opportunity for theoretical consistency test. On the other hand, the small error in attenuation caused, for instance, by structure could lead to the large errors in ζ -potential. That is why we use the other design of the CVI sensor, which we call ‘ ζ -potential probe’. Sensing electrodes are mounted on the surface of the ultrasound transducer which eliminates gap between transducer and electrodes. As a result $L = 0$ in Eq. (54) and attenuation influence disappears.

New theory yields a new range of the frequencies. This theory predicts that critical frequency becomes higher with increasing volume fraction. Computer computation shows that this shift is about one order of magnitude for volume fraction 40%. It means that optimum frequency range according to the new theory is

$$v/a^2 < \omega < 40v/a^2 \quad (55)$$

if we want to cover volume fractions up to 40%.

13. Materials and experimental protocol

We used silica Ludox and rutile R-746 from Dupont for this experiment.

Selection of the silica Ludox is related to the small size of these particles. It allows us to eliminate any particle size dependence in Eq. (54). Using small particles gives one more simplifying advantage: it eliminates the contribution of attenuation because small particles do not attenuate sound at low frequency. It means that the choice of small particles allows us to test volume fraction dependence only. It is important because this dependence is the most pronounced difference between different theories.

Silica Ludox TM satisfies all specified conditions because its nominal particle size reported by DuPont is approximately 22 nm. We measure the size using acoustics. It is quite close to the nominal value as it will be shown below. At the same time particle size should not be too small for the given ionic strength in order

to satisfy the thin double layer restriction. Silica Ludox meets this requirement because of the relatively high ionic strength of approximately 0.1 mol/l. Otherwise we would have to generalize the theory removing thin double layer restriction following Babchin et al. [58,59].

The selection of rutile as the second dispersion gives us an opportunity to test particle size dependence and enhance the density contrast contribution. We used rutile R-746 produced by E. I. DuPont de Nemours. This product was a concentrated stable dispersion with weight fraction of solids 76.8% wt. We took 100 ml of this dispersion and weighed it. This weight was 234 g which yields particle material with an average density of 3.9 g/cm³. This density was somewhat lower than density of the regular rutile, perhaps, because of the stabilizing additives.

The equilibrium dilution protocol requires a pure solvent which is identical to the medium of the given dispersed system. In principle one can try to separate the dispersed phase and dispersion medium using either sedimentation or centrifugation. This method does not work for silica Ludox because the particle size is too small.

The other way to create an equilibrium solution for small silica Ludox is dialysis. We used this one. Dialysis allows us to equilibrate the dispersion medium with an external solution over some period of time. We used a regenerated cellulose tubular membrane Cell*Sept4 with a pore size of 12 000–14 000 Da. The external solution was KCl 10⁻¹ mol/l with pH adjusted to 9.5 using hydrochloric acid. The membrane filled with silica Ludox was placed inside of the KCl solution which was continuously mixed with the magnetic stirrer. We made two samples in order to check reproducibility.

In addition, we prepared another setup using KCl solution at pH 3. This setup allowed us to estimate the equilibration time. The initial pH of the silica Ludox is approximately 9 at 23°C. We monitor change in the pH of the external solution. The corresponding kinetic curve is shown in Fig. 3. It is seen that pH becomes 8.6 after 3 h of equilibration. It was close to the final pH value 8.7 after 12 days of equilibration. We waited 12 days because the equilibration time depends on the diffusion coefficient which is the highest for H⁺ ions. The higher the diffusion coefficient the lower the equilibration time.

Before starting the dilution we checked again the weight fraction of the silica Ludox using a pycnometer. We were concerned with losing silica particles through the membrane pores into the solution. The weight fraction remained unchanged which means that pores were too small for silica particles.

We had two sets of 50% silica with a corresponding equilibrium solution. It allowed us to check two ways of dilution. We used one set for diluting from the high weight fraction down. We did this adding solution to the dispersed system. We used the opposite procedure with the other sample. We added the dispersed system to the solution.

In the case of rutile we used centrifugation of the initial 76.8% wt. dispersion in order to create the equilibrium supernate. We used this supernate for preparing equilibrium 1.1% vol. rutile dispersion diluting the initial dispersion. After making the measurement with this dilute system we added more initial dispersion for

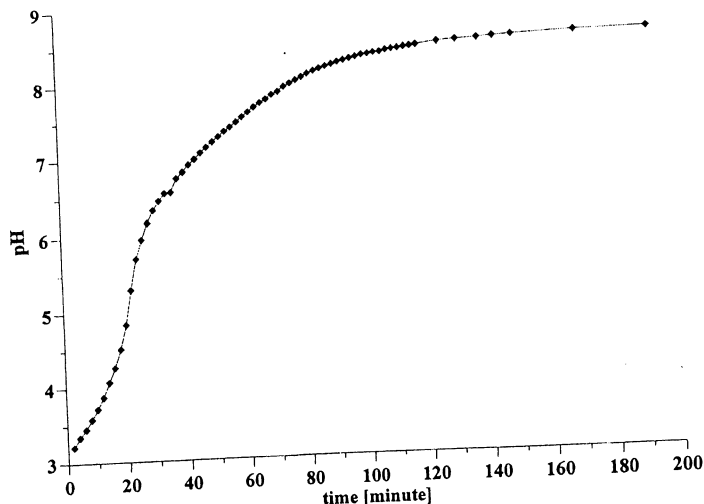


Fig. 3. Kinetic curve describing variation of the pH in the external dialysis solution vs. time for silica Ludox.

preparing the next volume fraction: 3.2% vol. We proceeded this way making a more and more concentrated system. All together 11 different volume fractions from 1.1 to 45.9% vol. were tested (see Fig. 5).

For each volume fraction we measured attenuation spectra, sound speed, pH, conductivity, temperature, magnitude and phase of CVI.

Attenuation spectra were measured within the frequency range from 3 to 100 MHz, sound speed at 10 MHz, conductivity at 3 MHz, magnitude of CVI at 3 MHz, phase of CVI at 1.5 MHz. Some of the results are discussed below.

14. Results and discussion

Measured attenuation spectra are shown in Figs. 4 and 5. It is seen that attenuation for silica Ludox is much lower than for rutile. It happens because of the smaller size and lower density contrast for silica. The attenuation spectra of silica becomes almost indistinguishable at a volume fraction above 9% which reflects a non-linear dependence of the attenuation on the volume fraction.

This peculiarity of the attenuation spectra was known before [9]. It is even more pronounced for rutile (Fig. 5). Attenuation at low frequency decreases with increasing volume fraction above 16.6% vol. It is exactly the same effect which makes attenuation constant for silica.

This non-linearity appears because of the particle–particle interaction. In the absence of the particle–particle interaction contribution of the particles to the

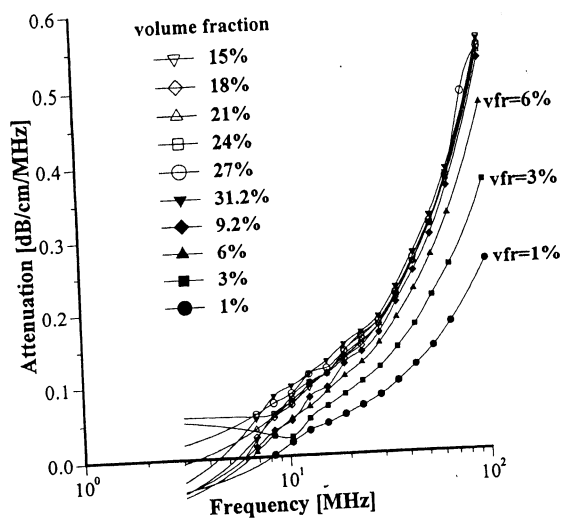


Fig. 4. Attenuation spectra measured for silica Ludox TM at different volume fractions.

total attenuation is additive. As a result attenuation is a linear function of the volume fraction like in the ECAH theory, for instance. Particle interaction affects dissipation of the acoustic energy caused by each particle. Their contribution to the total attenuation is not proportional to their volume any more but depends on the presence of other particles and interparticle distance. This dependence on the interparticle distance brings a new term to the volume fraction dependence and shifts the critical frequency to the higher values.

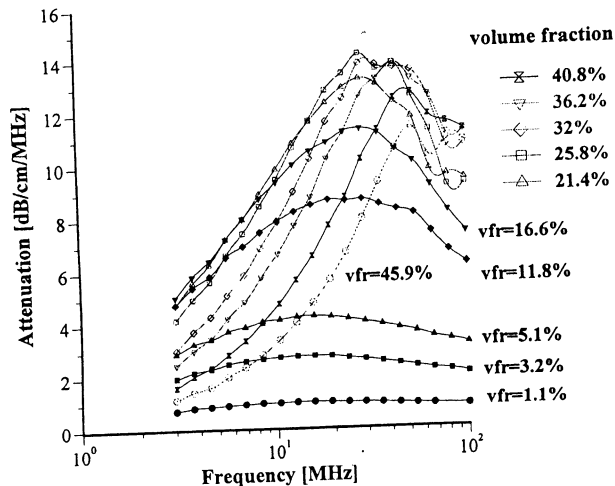


Fig. 5. Attenuation spectra measured for rutile R-746 at different volume fractions.

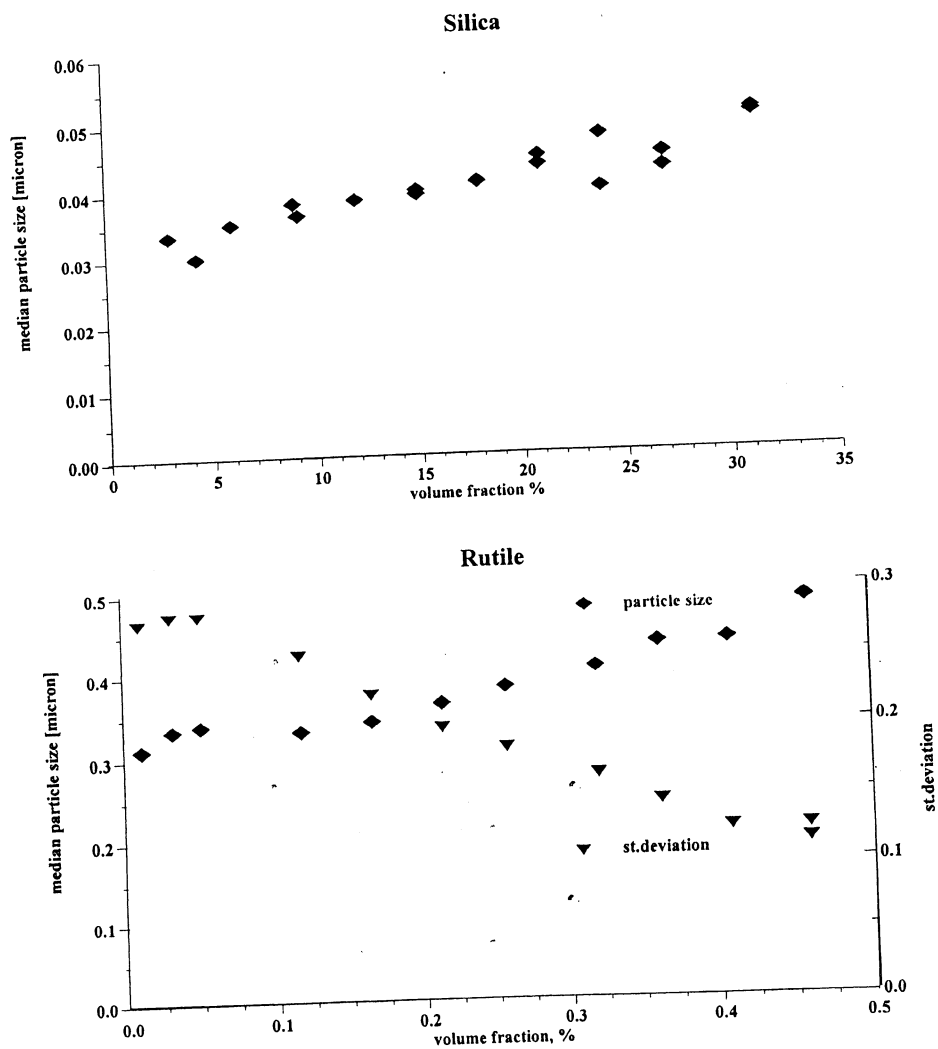


Fig. 6. Median particle size of the silica and rutile calculated from the attenuation spectra of Figs. 4 and 5.

Our theory presented above takes into account particle–particle interaction and as a result particle size calculated from this attenuation spectra is almost constant for all volume fractions for both silica and rutile (Fig. 6). A slight increase at a high volume fraction can be caused by aggregation. It is important to mention here that the dilute case theory would yield size decreasing dramatically with volume fraction.

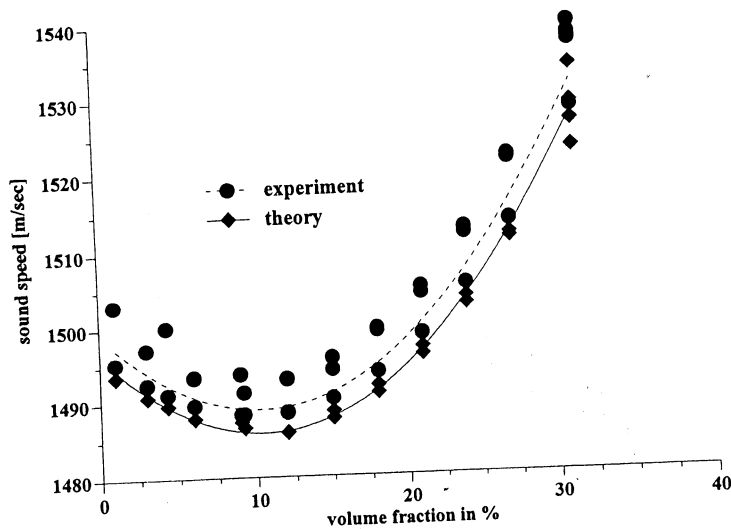


Fig. 7. Sound speed of the silica Ludox TM vs. volume fraction measured and calculated.

It is seen that our size is somewhat larger than nominal. Perhaps, the difference in the nominal value is caused by a different technique applied by Dupont for characterizing size of these particles. It is also clear that nominal size corresponds to the dilute system whereas we measured size for the concentrated one.

It is seen (Fig. 4) that attenuation for silica at 3 MHz is negligible indeed. It means that our expectations to eliminate this contribution to the CVI measurement using small particles were true.

At the same time we have appreciable attenuation for rutile at 3 MHz. This gives us a chance to verify the way we correct CVI for sound attenuation [Eq. (54)].

Sound speed of the silica Ludox dispersion varies only within 2% for weight fraction changing from 1 to 50% (see Fig. 7). It eliminates contribution from the changing of the acoustic impedance to the measured CVI for silica as well.

Figs. 8 and 9 illustrate ζ -potential values calculated from the measured CVI using various theoretical models. You can see that only our new theory yields a ζ -potential which remains almost the same within the complete volume fraction range. Variations do not exceed 10%.

At the same time 'hybrid O'Brien's theory' produces a big drop in the ζ -potential at a high volume fraction. This theory is the combination of O'Brien's relationship and our cell model theory for dynamic electrophoretic mobility. In the case of rutile the error reaches 300% at a volume fraction of 45.9%.

Similar results for silica allow us to conclude that the reason for this erroneous ζ -potential drop is the O'Brien relationship but not our theory for dynamic mobility. Our theory reduces in this case to the Smoluchowski law. It is the O'Brien relationship which brings about a 100% error in ζ -potential for silica at 30% vol.

The situation becomes even worse for the original O'Brien's theory combined with the Levine cell model. In principle we are able to apply the original O'Brien's

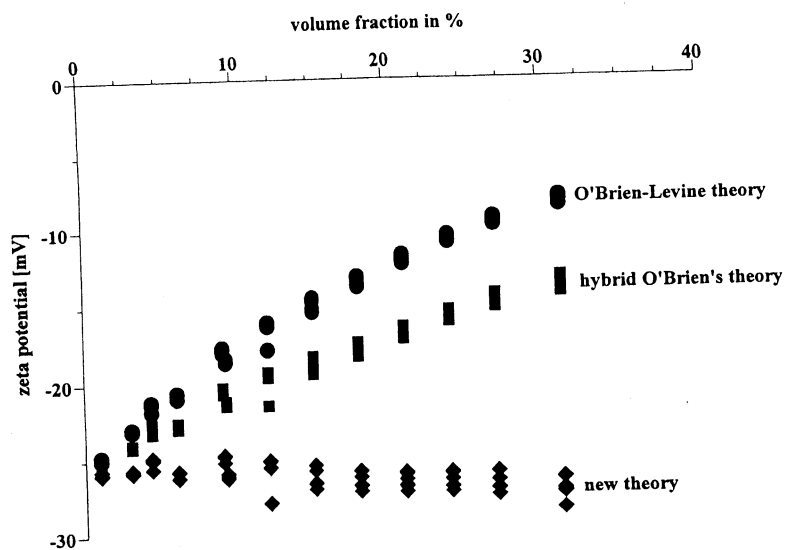


Fig. 8. Electrokinetic ζ -potential calculated from the measured CVI at various volume fractions using different electroacoustic theories for silica Ludox.

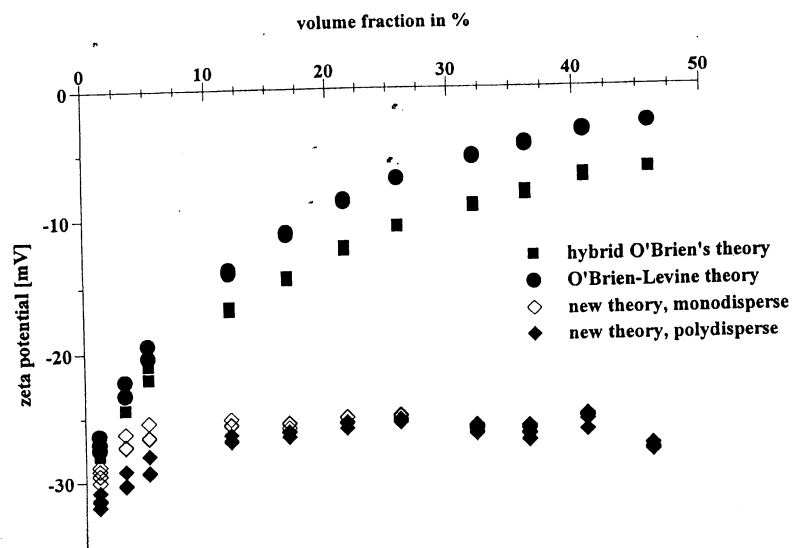


Fig. 9. Electrokinetic ζ -potential calculated from the measured CVI at various volume fractions using different electroacoustic theories for rutile R-746 from Dupont.

theory as it is presented in the patent [46] with the Levine cell model. However, instead of recovering these complicated mathematical expressions we decided just to show the effect of the missing volume fraction dependence. It is known [27] that the Levine cell model lacks the multiplier K_s/K_m compared to the Shilov-Zharikh cell model [25,26]. This difference is a major factor distinguishing the 'O'Brien-Levine theory' and 'hybrid O'Brien theory' theories for this particular dispersion. These theories have different particle size dependence but in this case of relatively small particles this difference is not very important. Though, we neglect difference in particle size dependence and take into account only different volume fraction effect. The last curves marked as the 'O'Brien-Levine theory' illustrates a result produced by this theory within the scope of the mentioned above assumption of the same particle size dependence for two theories.

15. Applications

It is impossible to give a complete list of all potential applications for acoustics and electroacoustics. The fact that these techniques are suitable for concentrated systems makes almost any real dispersed system of both natural and man made origins a potential object for these techniques. We give here only several major applications which can illustrate the power of this new characterization technology. Information about precision and accuracy is available in the paper [10].

16. Ceramics and other solid particles in liquids

Determination of both the particle size distribution and the zeta potential of ceramic slurries is of key importance in optimizing performance. The particle size of the slip is closely related to inhomogeneities, which in turn relates to fracture origins as well as shape distortion/cracking during drying, pyrolysis and sintering. Furthermore, the zeta potential of the slurry particulates can be used as a tool for optimizing chemical dosage to achieve the desired colloid stability and size distribution.

Traditional measurements of particle size and zeta potential usually involve light scattering or sedimentation techniques and require extreme dilution of the ceramic slip. This dilution step often changes both the size distribution and the zeta potential of the sample, thereby distorting the very information being sought. Characterizing the concentrated sample directly would allow a more realistic picture of the true agglomeration status and aid in the optimization of the dosage of various chemical additives in situ. In contrast, measurements of the diluted samples with traditional methods often reveals only the primary size of the raw materials. Preparation steps used in dilution, chemical modification, stirring, and sonication can break up agglomerations and destroy useful information about the original slurry.

Acoustic spectroscopy can provide accurate particle size data even in concen-

Table 4
Median particle size in microns of Aluminas Sumitomo

	Acoustics, DT-1200	Manufacturer (Method unknown)
AKP-15	0.684	0.7
AKP-30	0.319	0.3
AKP-3000	0.520	0.5
AA-2	1.956	2

trated slurries [60–62]. Fig. 10 shows the measured attenuation spectra and corresponding particle size distribution for four different alumina slurries. Table 4 gives a comparison of the measured particle size with the manufacturer's data derived from traditional methods.

The agreement between acoustic and traditional methods is quite good because care was taken in formulating the concentrated dispersion with an optimum level of surfactant to ensure good dispersion of the primary particles. In many real-world cases, the final dispersant dose may have been simply extrapolated from very dilute measurements and one may obtain a larger particle size in the actual slurry than predicted from these dilute measurements of the raw materials. It is almost always better to characterize the particle size of the slurry. When this does not compare with dilute measurements one needs to examine whether the chemical formulation is adequate.

Acoustic spectroscopy is applicable to virtually all ceramic materials. Fig. 11 shows typical particle size distributions for a variety of commonly used ceramic materials. For many applications it is important to recognize particle size sub-populations in the final slurry. Such bimodal distributions might result from agglomeration of primary particles caused by non-optimum dispersant addition, or in the following example, from an intentional addition of a second size fraction. Fig. 12 shows the acoustic attenuation spectra for three 10 vol. % alumina slurries: a 0.36- μm sample; a 2- μm sample; and a 1:1 mix of the two. The theoretical spectra fit quite precisely the experimental data giving high confidence in the results. Fig. 12 shows the resulting size distributions for the two single component slurries (blue and black curves) as well as the bimodal distribution for the mixed slurry (red curve).

In many ceramic applications the ceramic slip is actually a mixture of more than one solid component. Traditional optical or sedimentation techniques cannot provide correct interpretation of such mixtures and typically assume that all particles have a common set of physical properties. In contrast, commercially available software for acoustic spectroscopy has evolved to the point that allows the specification of at least two classes of disperse particles. For example, Fig. 13 shows an example of a mixed system of alumina and zirconia particles. This figure shows the attenuation spectra for three 5 vol.% slurries: a 2- μm single component alumina; a 0.3- μm single component zirconia; and a 1:1 mix of the two ingredients.

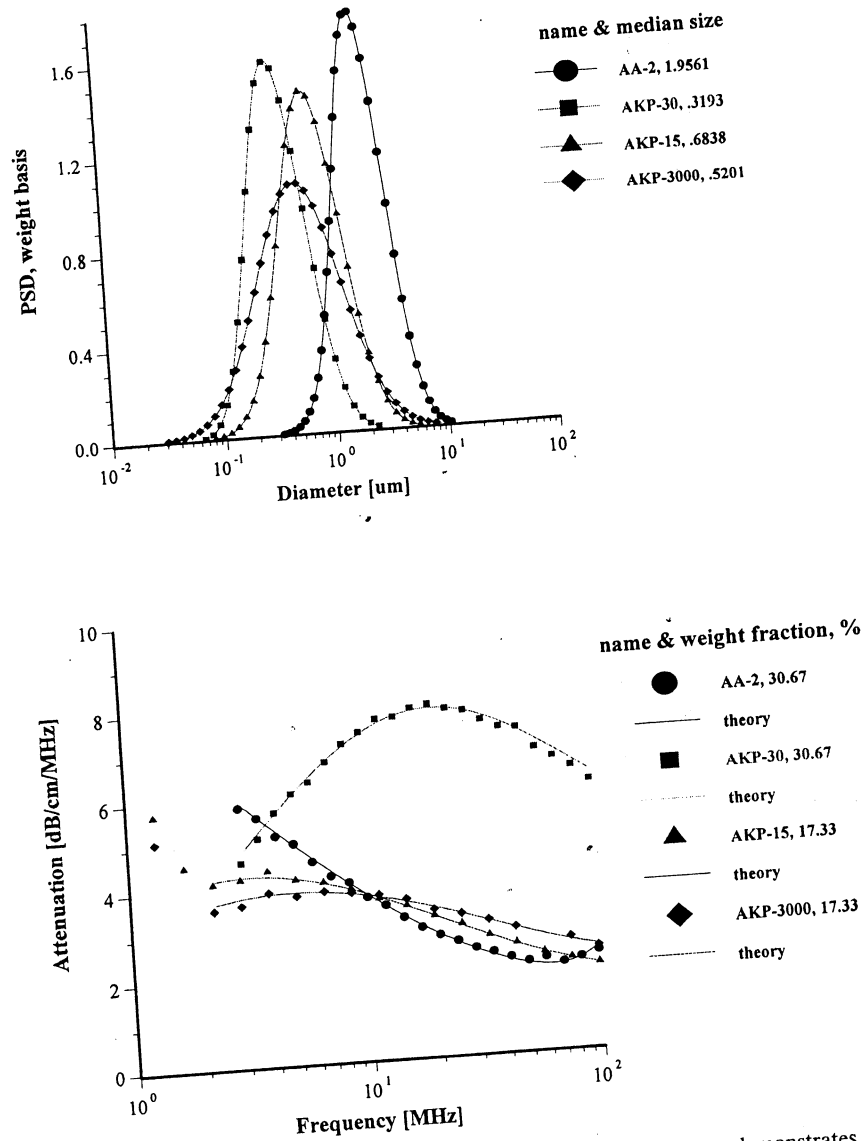


Fig. 10. Measured particle size distributions for four Sumitomo aluminas demonstrates the wide particle size range capability of acoustic spectroscopy and the ability to provide quality control of a wide range of raw materials. Acoustic Spectra for same four aluminas fit precisely with theoretical curve based on output particle size distribution.

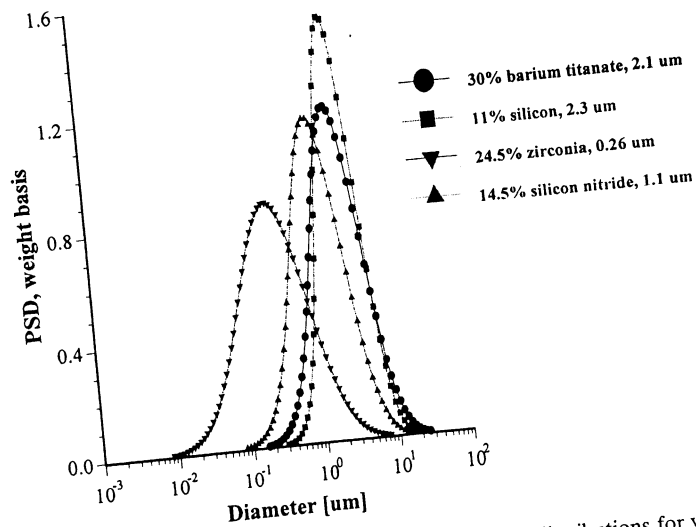


Fig. 11. Versatility of acoustic method is illustrated by particle size distributions for variety of ceramic materials.

Again, the theoretical spectra fit the experimental data quite well giving high confidence in the results. Fig. 13 shows the resulting single mode particle size distribution for each oxide measured separately, as well as two separate single mode distributions measured for each component in the mixed slurry system.

It is not always appreciated that the particle size distribution of a slurry is not simply a function of the primary size of the constituent ingredients, but instead is a result of many complex chemical and mechanical operations on the system. The zeta potential of the system is one parameter that can be used to investigate this complex relationship. Fig. 14 compares zeta potential data for a typical rutile and alumina sample using electroacoustic data. The pH at which the zeta potential goes to zero is referred to as the isoelectric pH. Different materials may have quite different isoelectric points as is evident from this figure. If we desire good stability, then we need to operate far enough from the isoelectric point to achieve a zeta potential in excess of 20–30 mV, either plus or minus. For the alumina presented in Fig. 14, the optimum stability for this alumina, is outside of the pH range between 8 and 11 where the zeta potential is less than 20 mV. This complex relationship between zeta potential and particle size distribution can be easily understood using acoustic spectroscopy.

In the real world, the situation is sometimes even more complex. The particle size and zeta potential is not just a function of the final chemical state of the system, but may also depend on the history of how the system reached this state. In other words, the complete history of the sample may be important as is illustrated in Fig. 14, a case history of a plant manufacturing silicon nitride. The red curve

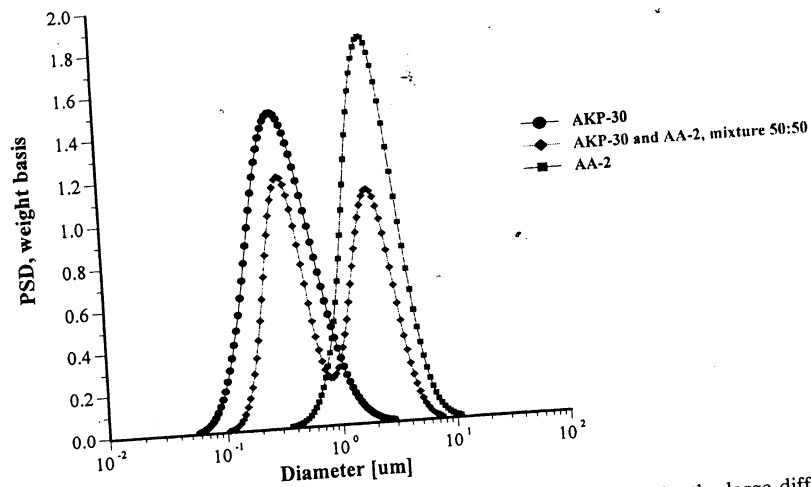
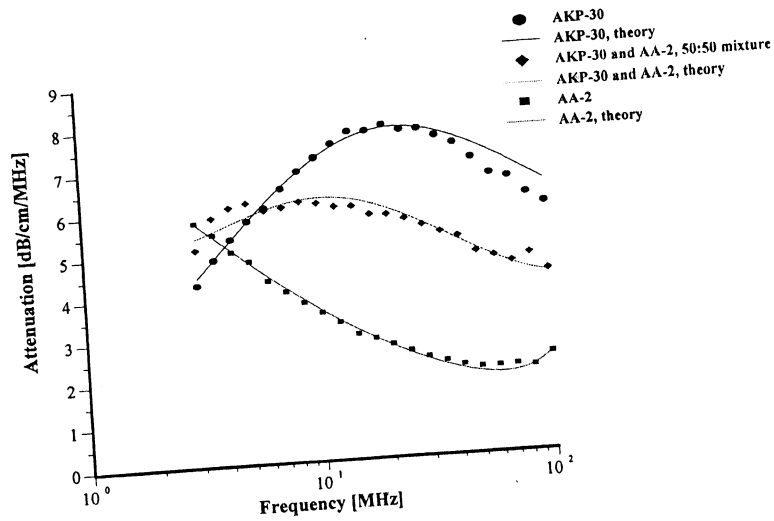


Fig. 12. The high sensitivity of acoustic attenuation spectra is illustrated by the large difference in the attenuation spectra for two different size alumina slurries as well as a 1:1 mixture of each. The validity of the theory is established by the good fit between the theoretical prediction and the experimental data. Each peak in the bimodal distribution for the mixed slurry agrees precisely with a corresponding peak in the size distribution for the single component slurry.

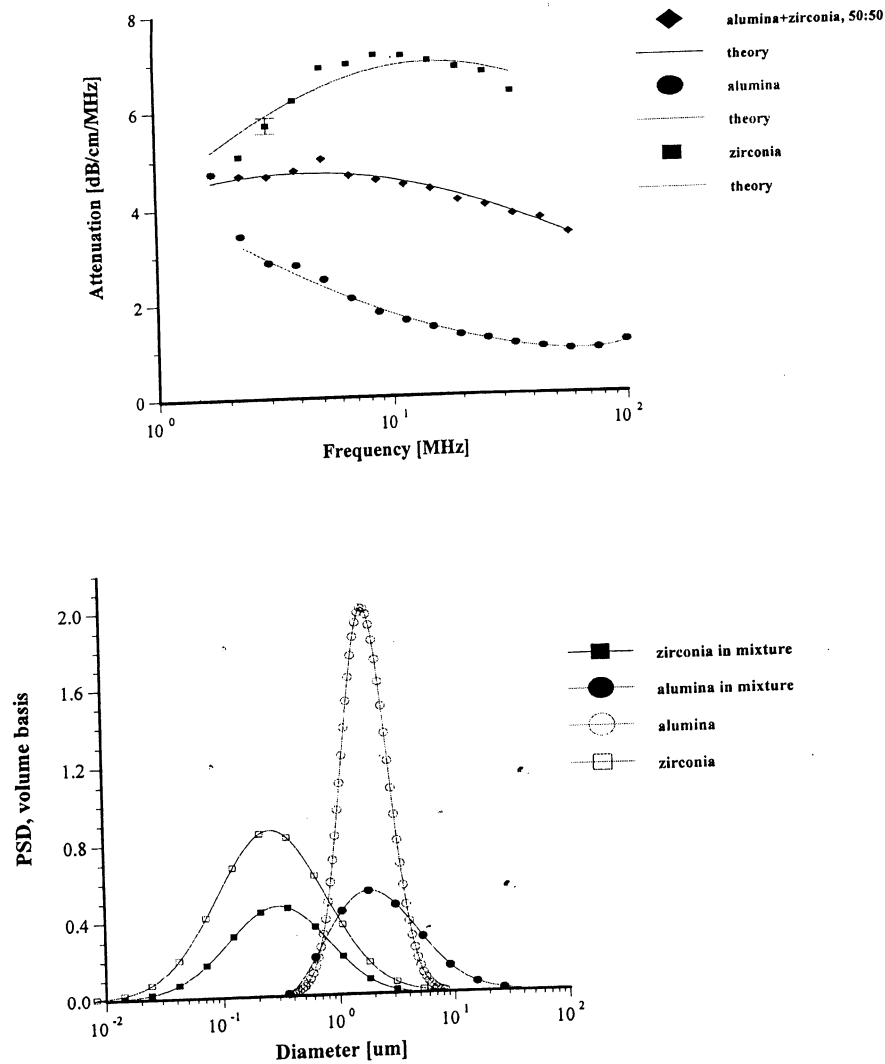


Fig. 13. The attenuation spectra for alumina, zirconia, and 1:1 mixture shows that three cases have quite different spectra and that best-fit theoretical distribution find good solution for each case. Particle size distribution for each component in mixed slurry can be measured. The size distribution for each component in the mixed slurry agrees well with the particle size for each component measured separately.

shows the zeta potential as the pH is decreased to an acid condition. From just this data alone one would think that a pH of 7–8 would provide adequate zeta potential for stability. However, operating experience in the plant indicated otherwise. A clue to the problem was found by reversing the titration towards more alkaline

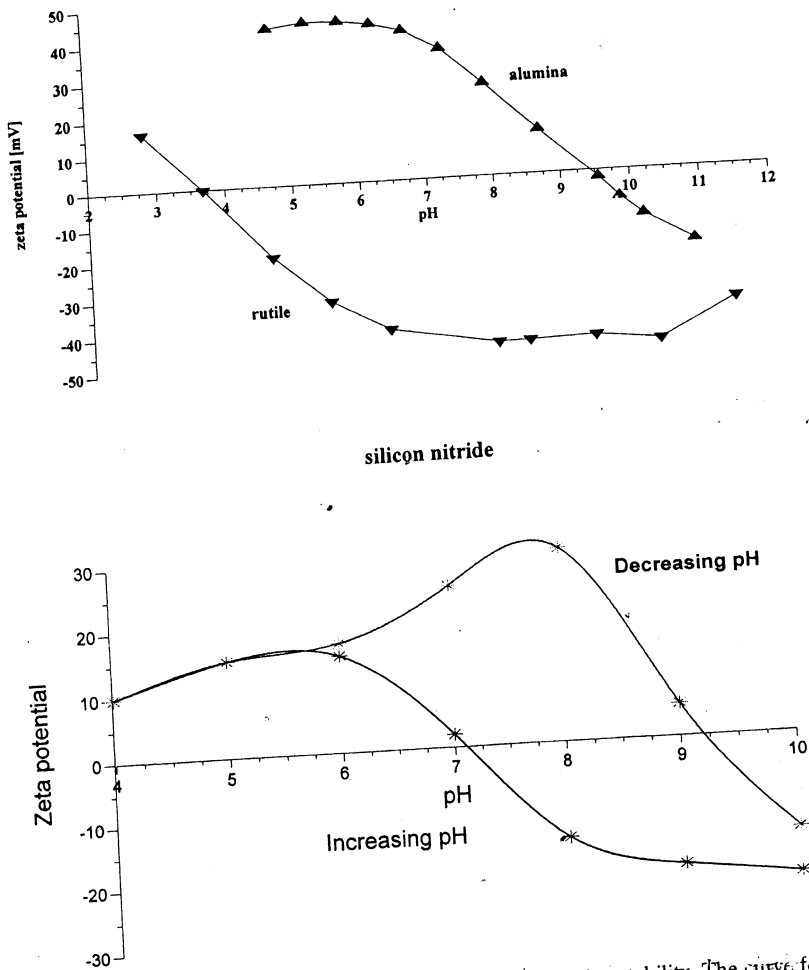


Fig. 14. The slurry isoelectric point suggests optimum pH for achieving stability. The curve for alumina slurry suggests avoiding the pH range 9-10, whereas the titania curve suggests avoiding the range pH 3-4. Slurry stability depends not only on chemical state but how one reaches this state. Titration of production silicon nitride to low pH indicates high zeta potential and good stability at pH 7-8. However, process engineers found that this pH did not provide good operating performance. Actual process included an acid wash of slurry. Back titration to alkaline conditions shows a dramatic shift in isoelectric point requiring shift in plant operating conditions.

conditions. The reverse titration, shown by the blue curve, revealed that the isoelectric point decreased by 2 pH units after the slurry was exposed to this acid condition. Investigation of plant operations showed that the slurry processing normally included such an acid wash. In order to obtain adequate stability following this acid condition, the data suggests that the process pH must be

readjusted to a point either significantly below or above this new isoelectric point. But how can we explain this dramatic shift in the isoelectric point? The explanation is actually quite simple. The initial slurry had a very small level of contamination, which was insignificant in terms of the overall stability of the system. However, under acid conditions this minor component dissolved. Upon subsequent change to more alkaline conditions, this dissolved material re-precipitated on the surface of the major silicon nitride component. Now this minor component, although present only in seemingly insignificant quantities, nevertheless dominated the surface chemistry of the silicon nitride material. By realizing that the final state is dependent on the history of the sample the process could be modified to accommodate this change.

Modern chemical–mechanical polishing materials (CMP) present another challenge for measuring techniques. Certain aspects of this application cause difficulties when using instruments based on traditional techniques. The particle size of a typical CMP slurry is too small for sedimentation-based instruments or electric zone instruments. Typically, the mean size of CMP materials is approximately 100 nm with very few particles larger than 500 nm. The range in the size of the particles may be greater than 1000:1 which also eliminates many classical techniques. CMP systems are also typically shear sensitive. Shear caused by the polishing process itself or the delivery system may cause unpredictable assembly of the smaller particles into larger aggregates. However, these aggregates may be weakly formed and easily destroyed by subsequent sonication, high shear, or dilution. Therefore, any technique which requires dilution or other sample preparation steps may destroy the very aggregates that one is attempting to quantify by measurement. Therefore, the CMP systems must be characterized in its natural state, without any dilution or sample preparation.

One feature of acoustic spectroscopy which thus far has not been described sufficiently in the literature is the ability to characterize a bimodal PSD. Although Takeda et al. [62] demonstrated that acoustic spectroscopy is able to characterize bimodal distributions of mixed alumina particles, the ultimate sensitivity in detecting one very small sub-population in combination with another dominant mode has not yet been investigated. The ability to recognize a small sub-population is critical for CMP studies as indicated in the literature.

Unfortunately, there is no agreement in the literature as to the number of larger particles which might be allowed in a CMP slurry. If it is assumed that only one large particle of 1 μm size be allowed per 100 000 small 100-nm particles, the target sensitivity corresponds to large particles amounting to 1% of the total weight of all particulates.

The acoustic spectrometer does not directly measure particle size, but measures an attenuation spectra and calculates the particle size assuming a certain model for describing the sound attenuation in terms of the physical properties of the system. It follows therefore, that this target sub-population sensitivity needs to be translated into a corresponding precision and accuracy specification for the attenuation measurement. It was determined from a theoretical standpoint, that the required precision is roughly 0.01 dB/cm/MHz [63]. The set of experiments were per-

Table 5
Median particle size for various silica samples

	Manufacturer	Acoustics
Ludox-TM	22 nm (area basis)	30 nm (weight basis)
Geltech 0.5	0.5 μm	0.65 μm
Geltech 1.5	1.5 μm	1.72 μm
Cabot SS12		63 nm
Cabot SS25		62 nm

formed with a single component system of Dupont silica Ludox-TM to confirm that the DT-1200 acoustic spectrometer indeed meets this target requirement.

A second set of experiments was then made to test whether the attenuation spectra changed the reproducibly when a small amount of the larger particles was added to a single component slurry of smaller particles. Two slurries were used for the small particles: Ludox-TM and Cabot SS25. Two Geltech silica with nominal sizes of 0.5 and 1.5 μm were used as the model large particles. It was found that the change in the attenuation spectra was statistically significant when the large particles amounted to at least 2% of the total weight of all particulates. Expressed another way, the detection limit for this 12 wt.% slurry corresponded to a sub-population which was only 0.24 wt.% in terms of the total sample weight, or 0.24 g of large particles per 100 g of the slurry.

The attenuation spectra and corresponding PSD for all five single component silica slurries is presented in Fig. 15. These tests allowed us to compare the particle size determined by acoustic spectroscopy for the five 12 wt.% test slurries with independent data from the manufacturers. The values of the median size in each case is given in Table 5. It is interesting to note that there is some difference between the acoustically measured data and that provided by the manufacturer. In large part this is related to differences in the characterization technique. For instance, the size of the Ludox-TM slurry is determined by Dupont using a titration method. This method yields an average size on an area basis. Acoustic spectroscopy gives us a size on a weight basis, which for a polydisperse system will always be somewhat larger than an area-based size. In addition, acoustic spectroscopy implies some assumption about the real dispersed system when particle size is being calculated from the attenuation spectra. These assumptions and variation in physical properties which are involved in the calculations can cause some variation in size as well.

In order to test the ability of acoustics to correctly determine bimodal PSD, Ludox TM or CMP SS12 small particles were used as the major component of a slurry. The Geltech 0.5 or Geltech 1.5 were used as 'large' and 'larger' particles in the minor component of the mixed slurry. In each case the minor fraction was added to the Ludox-TM or the CMP SS12 systems in steps. Each addition increased the relative amount of the larger particles by 2%. The attenuation spectra was measured twice for each mixed system in order to demonstrate reproducibility.

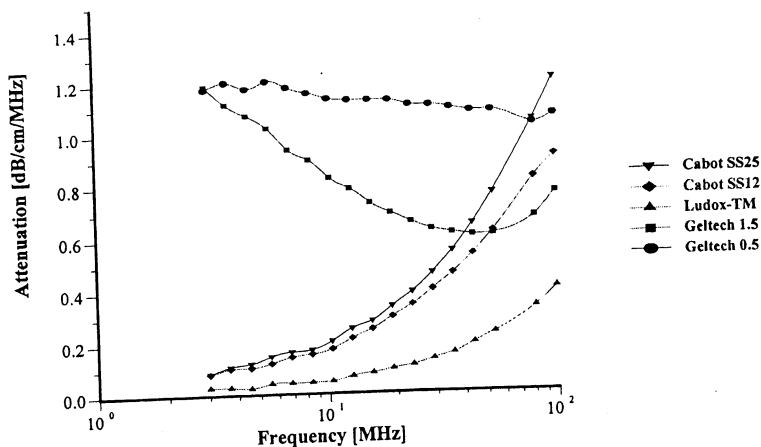


Fig. 15. Attenuation spectra measured for Ludox TM silica, Geltech 0.5 and 1.5 silica, Cabot SS25 and SS12 silica. Total solid content is 12 wt.% except for SS25 which is 25 wt.%. Particle size distributions corresponding to the measured attenuation spectra.

Fig. 16 illustrates the results of these mixed system tests. It is seen that attenuation increases with higher concentrations of the 'large' or 'larger' particles. The increase in the attenuation with increasing doses of the Geltech content is in all cases significantly larger than the precision of the instrument. This demonstrates that the DT-1200 data contains significant information about the small amount of large particles.

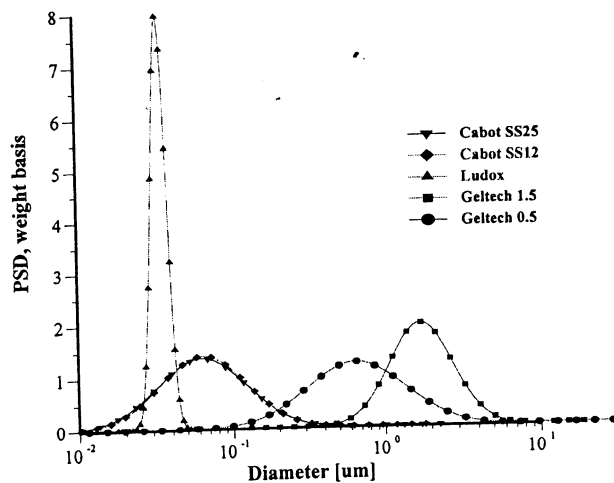


Fig. 16. Attenuation spectra and corresponding particle size distribution for Cabot SS25 silica diluted down to 12 wt.% with various additions of Geltech 0.5 silica. Total solid content is 12 wt.%. The legend shows the fraction of the total solid content corresponding to the silica Geltech.

The final question is to determine whether the calculated PSD calculates a correct bimodal distribution for these mixed model systems. The DT-1200 always calculates a log-normal and a bimodal distribution which best fits the experimental data. These two PSD are best in the sense that the fitting error between the theoretical attenuation calculated for the best PSD and the experimental attenuation is minimized. These fitting errors are important criteria for deciding whether the log-normal or bimodal PSD is more appropriate for describing a particular sample. For instance, the PSD is judged to be bimodal only if the bimodal fit yields substantially smaller fitting error than a log-normal PSD. It was shown that fitting errors for the bimodal PSD was better than the log-normal for all of the mixed systems over the whole concentration range and for both the large and larger sized particles. According to the fitting errors, all PSD in the mixed systems are bimodal, which is correct for these known mixed systems. Details about error analysis implemented into the DT instruments software are described in the paper [10].

Acoustics yields information only about particle size and for CMP slurries information about ζ -potential is very valuable for proper characterization of these materials. Electroacoustics opens the way to perform this characterization with very high quality of reproducibility and speed. Fig. 17 shows results of pH titration of silica Ludox and CMP slurry produced by ECC. It is seen that electroacoustics is able to characterize ζ -potential below 1 mV with a precision of approximately 0.1 mV. This degree of accuracy and precision exceeds results obtainable with micro-electrophoresis.

17. Emulsions, microemulsions and latex

There are many instances of successful characterization of the particle size distribution and zeta (ζ) potential of emulsion droplets. There are two quite representative reviews of these experiments published by McClements [4] (acoustics) and Hunter [12] (electroacoustics).

We present here results of some recent investigations of the various factors that affected stability, size and ζ -potential of the emulsion droplets. One of the most important parameters that affects emulsions is the surfactant concentration. Fig. 18 illustrates this for 6% by weight reverse water-in-oil emulsion. The oil phase was simply commercially available oil diluted twice with paint thinner in order to reduce the viscosity of the final sample. This figure shows the attenuation spectra for the three samples. The pure oil phase sample exhibited the lowest attenuation. It is important to measure the attenuation of the pure dispersion medium when a new liquid is evaluated. In this particular case, the intrinsic attenuation of the oil phase was almost 150 dB/cm at 100 MHz which is more than seven times higher than for water. This intrinsic attenuation is a very important contribution to the attenuation of ultrasound in emulsions. It is the background for characterizing emulsion systems.

The emulsion without any added surfactant was measured twice with two different sample loads. As the water content was increased the attenuation became

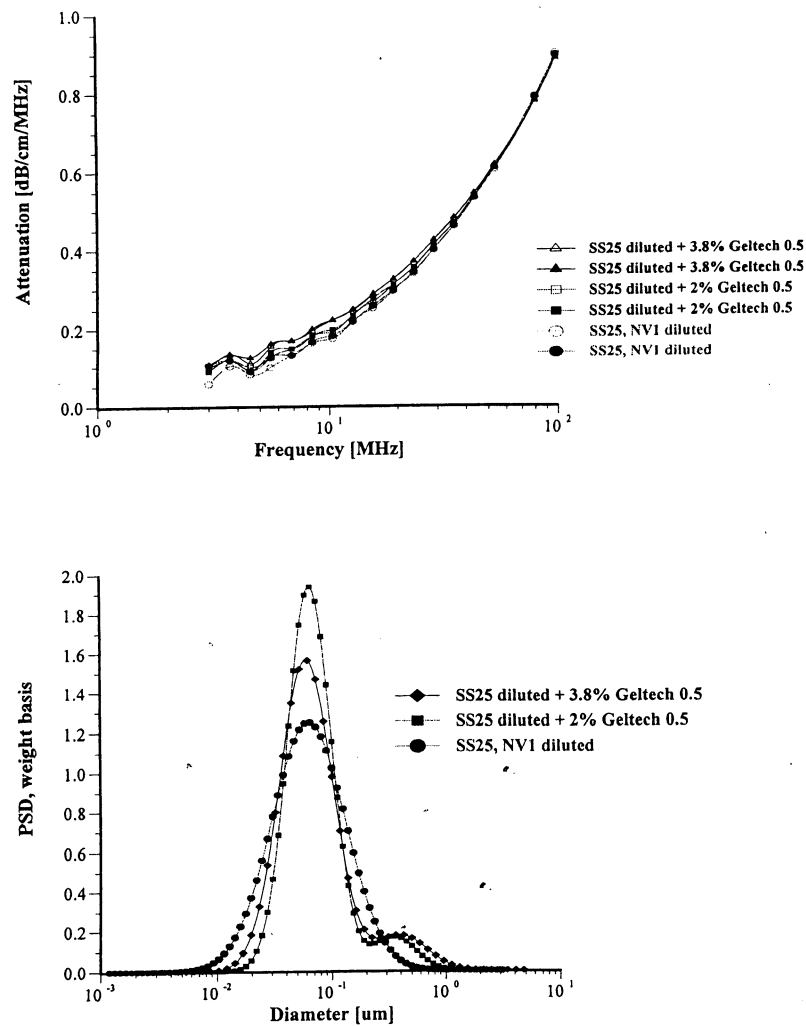


Fig. 17. Titration of silica Ludox TM at 10% wt. and chemical-mechanical polishing silica ECC.

greater in magnitude. For this system, the attenuation was found to be quite stable with time. Addition of 1% by weight AOT (sodium bis 2-ethylhexyl sulfosuccinate) changed the attenuation spectrum dramatically. This new emulsion with modified surface chemistry was measured twice in order to check reproducibility. The corresponding particle size distribution is shown in Fig. 18 and indicates that the AOT converted the regular emulsion into a microemulsion as one could expect.

These experiments proved that the acoustic technique is capable of characterizing the particle size distribution of relatively stable emulsions. In many instances

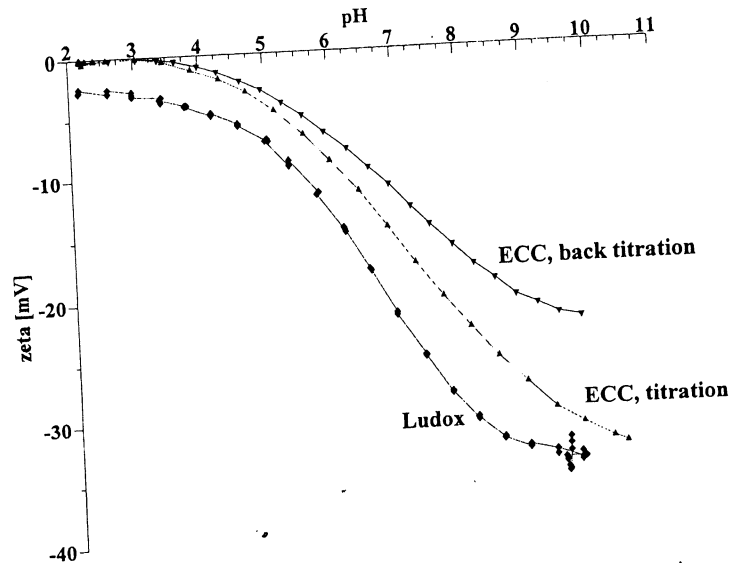


Fig. 18. Attenuation and corresponding particle size distribution of 6% wt. water-in-car oil emulsion and microemulsion created by adding AOT.

emulsions are found not to be stable at the dispersed volume concentration required to obtain sufficient attenuation signals (usually above 0.5 vol.%). Hazy water in fuel emulsions (diesel, jet fuel, gasoline) may exist at low water concentrations of only a few 100 ppmv (0.01 vol.%) of dispersed water. Attempts at characterizing these systems without added surfactant resulted in unstable attenuation spectra. Water droplets were discovered to separate from the bulk emulsion and settle out on the chamber walls. This problem is less important for thermodynamically stable microemulsions which are discussed below following the paper [64].

The mixture of heptane with water and AOT is a classic three component system that has been widely studied due to a number of interesting features it exhibits. This system forms stable reverse microemulsions (water-in-oil) without the complication introduced by the addition of co-surfactant, such as alcohol, required by many other reverse microemulsion systems. This simplification makes the alkane/water/AOT system a model for studying reverse microemulsions.

There have been many attempts to measure the droplet size of this microemulsion. Several different techniques were used: PCS [65–70]; classic light scattering [67,69,70]; the neutron scattering SANS [72–74]; and SAXS [66,75,76]; ultracentrifugation [68,71,77]; and viscosity [66,68,71]. It was observed that the heptane/water/AOT microemulsions have water pools with diameters ranging from 2 nm up to 30 nm. The water drops are encapsulated by the AOT surfactant so that virtually all of the AOT is located at the interface shell. The size of the water droplets can be conveniently altered by adjusting the molar ratios of water to

surfactant designated as R ($[H_2O]/[AOT]$). At low R values ($R < 10$) the water is strongly bound to the AOT surfactant polar head groups and exhibits unique characteristics different from bulk water. At higher water ratios ($R > 20$), free water is predominant in the swollen reverse micellar solutions, and at approximately $R = 60$, the system undergoes a transition from a transparent microemulsion into an unstable turbid macroemulsion. This macroemulsion separates on standing into a clear upper phase and a turbid lower phase.

Despite all these efforts, there still remains questions regarding the polydispersity of the water droplets, and few studies are available above the R value of 60 where a turbid macroemulsion state exists.

Acoustic spectroscopy offers a new opportunity for characterizing these complicated systems. Details of this experiment are presented in the paper [64]. In all cases, the reported R values are based on the added water, and were not corrected for any residual water that may have been in the dried AOT or heptane solvent. Karl Fischer analysis of the AOT–heptane solutions before the addition of water resulted in an R value of 0.4. This amount was considered to be negligible.

Measurements were made starting with the pure water and heptane and then the AOT–heptane sample with no added water ($R = 0$). The sample fluid was removed from the instrument cell and placed in a glass bottle with a Teflon cap. Additional water was titrated and the microemulsion was shaken for 30 s before being placed back into the instrument cell. The sample cell contained a cover to prevent evaporation of the solvents. The samples were visually inspected for clarity and rheological properties for each R value. These steps were repeated for increasing water weight fraction or R ratios up to $R = 100$. At $R \geq 60$ the microemulsions became turbid. At $R > 80$, the emulsions became distinctly more viscous.

The weight fractions of the dispersed phase were calculated for water only without including the AOT. Each trial run lasted approximately 5–10 min with the temperature varied from 25–27°C. A separate microemulsion sample for $R = 40$ was made up a few days prior to the first study. For the $R = 70$ sample, a second acoustic measurement was made with the same sample used for the first study. The complete set of experiments for water, heptane, and the reverse microemulsions from $R = 0$ to 100 was repeated to evaluate the reproducibility.

Attenuation spectra measured in the first run up to $R = 80$ are presented in Fig. 19. The results for $R = 90$ and $R = 100$ are not reported because they were found to vary appreciably. As the water concentration is increased, the attenuation spectrum rises in intensity and there is a distinct jump in the attenuation spectrum from $R = 50$ to $R = 60$ in the low frequency range. This discontinuity is also reflected in the visual appearance as at $R = 60$ the system becomes turbid. The smooth shape of the attenuation curve also changes at $R > 60$. The stability and reproducibility of the system was questioned due to the irregular nature of the curve so the experiment at $R = 70$ was repeated and gave almost identical results. An additional experiment was run at $R = 40$ for a separate microemulsion prepared a few days earlier. This showed excellent agreement with the results for freshly titrated microemulsion. For R values > 70 , an increase in the viscosity and a decrease in the reproducibility of the attenuation measurement were observed.

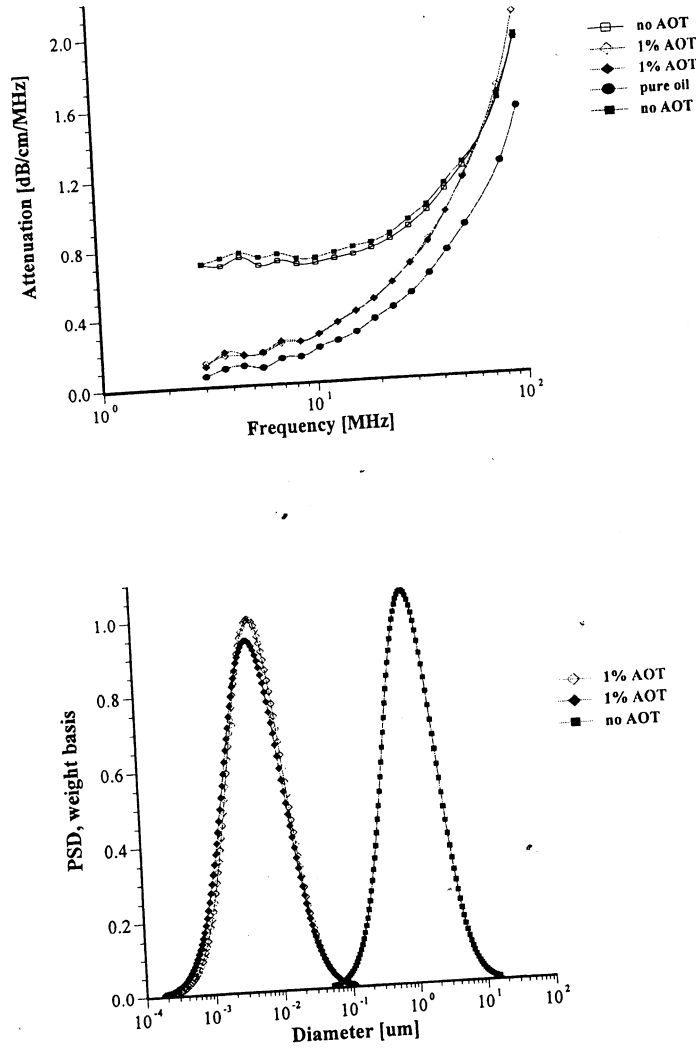


Fig. 19. Acoustic attenuation spectra measured for water/AOT/heptane system for different water to AOT ratios R .

This could be due to the failure of the model for this system as a collection of separate droplets at high R values.

The two lowest attenuation curves in Fig. 19 correspond to that of the two pure liquids: water and heptane. This attenuation is associated with oscillation of liquid molecules in the sound field. If these two liquids are soluble in each other, the total attenuation of the mixture would lie between these two lowest attenuation curves. But it can be seen that the attenuation of the mixture is much higher than

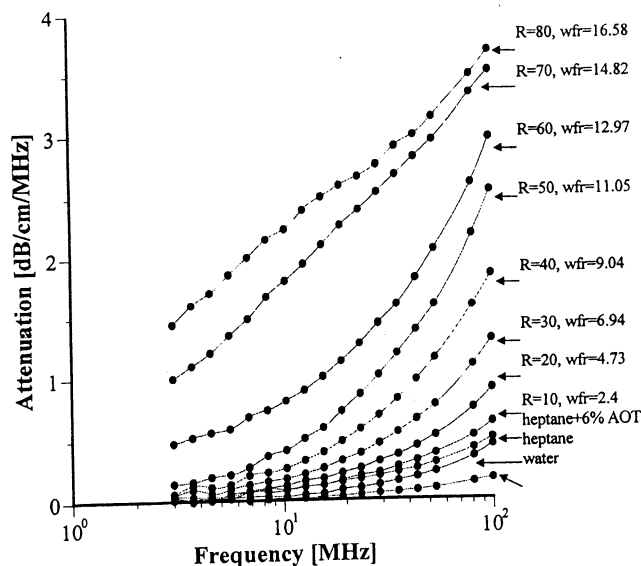


Fig. 20. Drop size distribution for varying $R[H_2O]/[AOT]$ from 10 to 50 and from 50 to 80.

that of the pure liquids. The increase in attenuation, therefore, is due to this heterogeneity of the water in the heptane system. The extra attenuation is caused by motion of droplets, not separate molecules. The scale factor (size of droplets) corresponding to this attenuation is much higher than that for pure liquids (size of molecules).

The current system contains a third component, AOT. A question arises on the contribution of AOT to the measured attenuation. In order to answer this question, measurements were done on a mixture of 6.1% wt. AOT in heptane ($R = 0$). It is the third smallest attenuation curve on Fig. 19. It is seen that attenuation increases somewhat due to AOT. However, this increase is less than the extra attenuation produced by water droplets. The small increase in attenuation is attributed to AOT micelles that are known to form without the addition of water. Unfortunately thermal properties of the AOT as a liquid phase are not known and the size of these micelles could not be calculated.

The particle size distributions corresponding to the measured attenuation spectra are presented in Fig. 20. It can be seen that the distribution becomes bimodal for $R \geq 60$ that coincides with the onset of turbidity. It is to be noted that such a conclusion could not easily be arrived at with other techniques. There is a feature

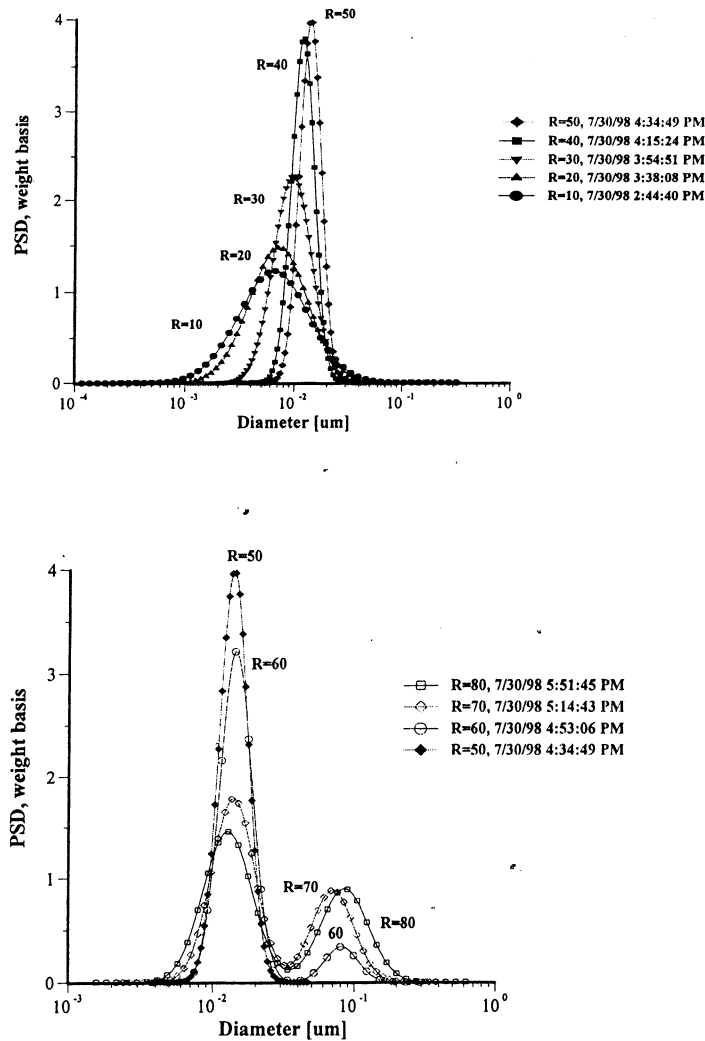


Fig. 21. Comparison of mean droplet size measured using acoustic spectroscopy, neutron scattering and X-ray scattering.

of this system, however, that can be compared with independent data from literature: mean particle size increases with R almost in a linear fashion. This dependence becomes apparent when the mean size is plotted as a function of R as in Fig. 21.

It is seen that the mean particle size measured using acoustic spectroscopy are in good agreement with those obtained independently using the neutron scattering (SANS) and X-ray scattering (SAXS) techniques (43,48,54) for R values ranging

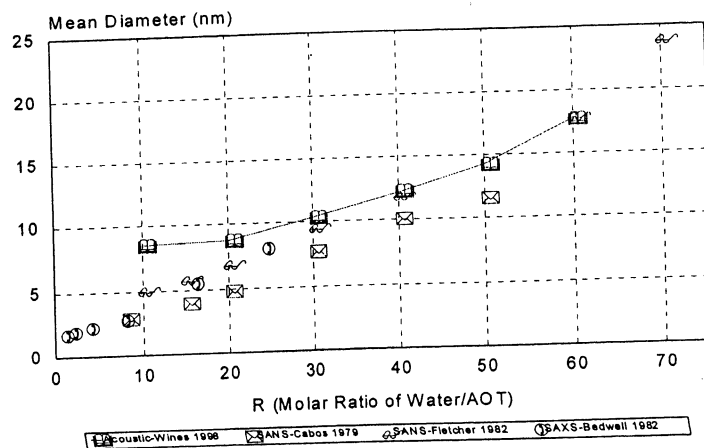


Fig. 22. Attenuation spectra for latex dispersions with different content of ethylene.

from 20 to 60. A simple theory based on the equi-partition of water and surfactant can reasonably explain the observed linear dependence.

At $R = 10$ the acoustic method gave a slightly larger diameter than expected. This could be due to the constrained state of the 'bound water' in the swollen reverse micelles. The water under these conditions may exhibit different thermal properties than the bulk water used in the particle size calculations. Also at the low R values ($R < 10$ or $< 2.4\%$ water), the attenuation spectrum is not very large as compared to the background heptane signal. Contribution of droplets to attenuation spectrum then may become too low to be reliably distinguished from the background signal coming from heptane molecules and AOT micelles.

There have been many successful experiments characterizing latex systems using both acoustics and electroacoustics. For instance, Allegra and Hawley [28] measured polystyrene latex. There is another successful application, this time with neoprene latex, which is described in the paper [33].

Successful examples of characterizing latex systems are possible only when thermal expansion coefficients are known. Unfortunately, this parameter is not known for many latex polymers. This problem becomes even more complicated for latex systems than for emulsions because the value of the thermal expansion depends strongly on the chemical composition of the polymer. Fig. 22 illustrates this fact for several ethylene copolymers with different ethylene contents. Variation of the ethylene content from 5 to 10% was found to cause significant changes in attenuation spectra. This change is associated with the thermal expansion coefficient, but not the particle size.

The uncertainty related with the thermal expansion coefficient makes latex systems the most complicated system for acoustics. This is important to keep in mind for testing a particular model of an acoustic instrument. Latex dispersions

that are used as standards for light-based methods should be used with caution as in many cases the thermal expansion properties of these standards are not well known.

18. Conclusions

In the last few years, the fields of acoustics and electroacoustics have made significant advancements in theoretical modeling, instrumentation, and experimental applications. The measurement of particle size by acoustic attenuation has been improved by new theoretical models that account for particle–particle interactions in concentrated systems. Refinements in the analysis of the different acoustic loss mechanisms have been presented in detail.

The combination of acoustic and electroacoustic spectroscopy provides more reliable and complete characterization of the disperse system than either one of those spectroscopes separately. Electroacoustic phenomena is more complicated when compared to acoustics because an additional electric field is involved. This problem becomes even more pronounced for concentrated systems and the best approach is to use acoustic attenuation to determine particle size, and electroacoustics separately to measure electric surface properties. The combined measurement of particle size and surface charge by the ESA technique requires a higher degree of theoretical complexity and can be less reliable.

New applications of the acoustic attenuation method and the colloid vibration current have been presented including ceramics, bimodal systems, chemical polishing materials, emulsions, microemulsions and latex systems. Further applications of these techniques are underway especially in the field of non-aqueous systems that cannot be easily studied by other methods. While theoretical models have made great advancements, more work is needed to explain why thermal effects seem to have little impact on the electroacoustics of emulsions, while acoustics is dominated by such effects.

Nomenclature

a :	Particle radius
b :	Cell radius
C_p :	Heat capacity at constant pressure
c :	Sound speed
Du :	Dukhin number
d :	Particle diameter
E :	External electric field
$\langle E \rangle$:	Macroscopic electric field strength
F_f :	Hydrodynamic friction force
K :	Conductivity attributed with index

I_r :	Local current in the cell
$\langle I \rangle$:	Macroscopic current
I :	Intensity of the sound
j :	Complex unit
h :	Special function (see Special functions)
H :	Special function (see Special functions)
l :	Complex wave number
l_r :	Cell layer thickness
L :	Gap in the electroacoustic chamber
M^* :	Stress modulus
N :	Number of the volume fractions
P :	Pressure
r :	Spherical radial coordinate
t :	Time
S_{exp} :	Measured electroacoustic signal
u :	Speed of the motion attributed according to the index
Z :	Acoustic impedance
α :	Attenuation specified with index
β :	Thermal expansion attributed with index
δ_v :	Viscous depth
δ_t :	Thermal depth
ϵ :	Dielectric permittivity of the media
ϵ_0 :	Dielectric permittivity of the vacuum
ϕ :	Electric potential
γ :	Hydrodynamic friction coefficient
η :	Dynamic viscosity
φ :	Volume fraction
κ :	Reciprocal Debye length
κ^σ :	Surface conductivity
λ :	Wave length
μ_d :	Dynamic electrophoretic mobility
ν :	Kinematic viscosity
θ :	Spherical angular coordinate
ρ :	Density attributed according to the index
τ :	Heat conductance attributed according to the index
ω :	Frequency
ζ :	Electrokinetic potential
Ω :	Drag coefficient
I :	Index of the particle fraction
p :	Particles
m :	Medium
s :	Dispersion
r :	Radial component
θ :	Tangential component
vis :	Viscous

th: Thermal
sc: Scattering
int: Intrinsic
in: Acoustic input
out: Acoustic output
rod: Delay rod properties

References

- [1] J.R. Pellam, J.K. Galt, Ultrasonic propagation in liquids: application of pulse technique to velocity and absorption measurement at 15 magacycles, *J. Chem. Phys.* 14 (10) (1946) 608–613.
- [2] C.T.J. Sewell, The extinction of sound in a viscous atmosphere by small obstacles of cylindrical and spherical form, *Philos. Trans. R. Soc. Lond.* 210 (1910) 239–270.
- [3] P.S. Epstein, R.R. Carhart, The absorption of sound in suspensions and emulsions, *J. Acoust. Soc. Am.* 25 (3) (1953) 553–565.
- [4] D.J. McClements, Ultrasonic characterization of emulsions and suspensions, *Adv. Colloid Interface Sci.* 37 (1991) 33–72.
- [5] Ultrasonic and Dielectric Characterization Techniques for Suspended Particulates, in: V.A. Hackley, J. Texter (Eds.), *The American Chemical Society, Ohio*, 1998.
- [6] J. Lyklema, *Fundamentals of Interface and Colloid Science*, vol. 1, Academic Press, 1993.
- [7] R.J. Hunter, *Foundations of Colloid Science*, Oxford University Press, Oxford, 1989.
- [8] H. Dhadwal, R. Ansari, W. Mayer, *Rev. Sci. Instrum.* 62 (12) (1991) 2963.
- [9] A.S. Dukhin, P.J. Goetz, Acoustic spectroscopy for concentrated polydisperse colloids with high density contrast, *Langmuir* 12 (21) (1996) 4987–4997.
- [10] A.S. Dukhin, P.J. Goetz, Characterization of aggregation phenomena by means of acoustic and electroacoustic spectroscopy, *Colloids Surf.* 144 (1998) 49–58.
- [11] P.J. Debye, *Chem. Phys.* 1 (1933) 13.
- [12] R.J. Hunter, Review. Recent developments in the electroacoustic characterization of colloidal suspensions and emulsions, *Colloids Surf.* 141 (1998) 37–65.
- [13] A.S. Dukhin, V.N. Shilov, H. Ohshima, P.J. Goetz, Electroacoustics phenomena in concentrated dispersions new theory and CVI experiment, *Langmuir* July 1999.
- [14] A.S. Dukhin, P.J. Goetz, Acoustic and electroacoustic spectroscopy, *Langmuir* 12 (19) (1996) 4336–4344.
- [15] T.A. Strout, Attenuation of sound in high-concentration suspensions, development and application of an oscillatory cell model, a thesis, The University of Maine, 1991.
- [16] U. Riebel, The fundamentals of particle size analysis by means of ultrasonic spectrometry, *Part. Syst. Charact.* 6 (1989) 135–143.
- [17] A.H. Harker, J.A.G. Temple, Velocity and attenuation of ultrasound in suspensions of particles in fluids, *J. Phys. D. Appl. Phys.* 21 (1988) 1576–1588.
- [18] R.L. Gibson, M.N. Toksoz, Viscous attenuation of acoustic waves in suspensions, *J. Acoust. Soc. Am.* 85 (1989) 1925–1934.
- [19] J. Happel, H. Brenner, *Low Reynolds Number Hydrodynamics*, Martinus Nijhoff Publishers, Dordrecht, The Netherlands, 1973.
- [20] A.S. Dukhin, V.N. Shilov, Yu. Borkovskaya, Dynamic electrophoretic mobility in concentrated dispersed systems. Cell model, *Langmuir* 15 (10) (1999) 3452–3457.
- [21] H.P. Pendse, T.C. Bliss, Han Wei, Particle shape effects and active ultrasound spectroscopy, in: V.A. Hackley, J. Texter, (Eds.), *Ultrasonic and Dielectric Characterization Techniques for Suspended Particulates*, American Ceramic Society, Westerville, OH, 1998.

- [22] Dispersion Technology Web Site www.dispersion.com
- [23] J. Happel, Viscous flow in multiparticle systems: slow motion of fluids relative to beds of spherical particles, *AICHE J.* 4 (1958) 197–201.
- [24] S. Kuwabara, The forces experienced by randomly distributed parallel circular cylinders or spheres in a viscous flow at small Reynolds numbers, *J. Phys. Soc. Jpn.* 14 (1959) 527–532.
- [25] V.N. Shilov, N.I. Zharkih, Yu.B. Borkovskaya, Theory of nonequilibrium electrostatic phenomena in concentrated disperse system. 1. Application of nonequilibrium thermodynamics to cell model, *Colloid J.* 43 (3) (1981) 434–438.
- [26] M.W. Kozak, J.E. Davis, Electrokinetic phenomena in fibrous porous media, *J. Colloid Interface Sci.* 112 (2) (1986) 403–411.
- [27] S. Levine, G.H. Neale, The prediction of electrokinetic phenomena within multiparticle systems. 1. Electrophoresis and electroosmosis, *J. Colloid Interface Sci.* 47 (1974) 520–532.
- [28] J.R. Allegra, S.A. Hawley, Attenuation of sound in suspensions and emulsions: theory and experiments, *J. Acoust. Soc. Am.* 51 (1972) 1545–1564.
- [29] J.D. McClements, Ultrasonic determination of depletion flocculation in oil-in-water emulsions containing a non-ionic surfactant, *Colloids Surf.* 90 (1994) 25–35.
- [30] D.J. McClements, Comparison of multiple scattering theories with experimental measurements in emulsions, *J. Acoust. Soc. Am.* 91 (2) (1992) 849–854.
- [31] A.K. Holmes, R.E. Challis, D.J. Wedlock, A wide-bandwidth study of ultrasound velocity and attenuation in suspensions: comparison of theory with experimental measurements, *J. Colloid Interface Sci.* 156 (1993) 261–269.
- [32] A.K. Holmes, R.E. Challis, D.J. Wedlock, A wide-bandwidth ultrasonic study of suspensions. The variation of velocity and attenuation with particle size, *J. Colloid Interface Sci.* 168 (1994) 339–348.
- [33] A.S. Dukhin, P.J. Goetz, C.W. Hamlet, Acoustic spectroscopy for concentrated polydisperse colloids with low density contrast, *Langmuir* 12 (21) (1996) 4998–5004.
- [34] A.S. Dukhin, T.N. Wines, P.J. Goetz, P. Somasundaran, *Acoustics and Electroacoustics for Emulsions*, Newsletter #4, <http://www.dispersion.com>, 1999.
- [35] L.W. Anson, R.C. Clivers, Thermal effects in the attenuation of ultrasound in dilute suspensions for low values of acoustic radius, *Ultrasonic* 28 (1990) 16–25.
- [36] M.A. Isakovich, *Zh. Exp. Theor. Phys.* 18 (1948) 907.
- [37] P.S. Waterman, R.J. Truell, *Math. Phys.* 2 (1961) 512.
- [38] R. Chanamai, J.N. Coupland, D.J. McClements, Effect of temperature on the ultrasonic properties of oil-in-water emulsions, *Colloids Surf.* 139 (1998) 241–250.
- [39] S. Temkin, Sound speed in suspensions in thermodynamic equilibrium, *Phys. Fluids* 4 (11) (1992) 2399–2409.
- [40] S. Temkin, Sound propagation in dilute suspensions of rigid particles, *J. Acoust. Soc. Am.* 103 (2) (1998) 838–849.
- [41] F. Booth, J. Enderby, On electrical effects due to sound waves in colloidal suspensions, *Proc. Am. Phys. Soc.* 208A (1952) 32.
- [42] J.A. Enderby, On electrical effects due to sound waves in colloidal suspensions, *Proc. R. Soc. Lond.* A207 (1951) 329–342.
- [43] B.J. Marlow, D. Fairhurst, H.P. Pendse, Colloid vibration potential and the electrokinetic characterization of concentrated colloids, *Langmuir* 4 (3) (1983) 611–626.
- [44] S.S. Dukhin, B.V. Derjaguin, Electrokinetic phenomena, in: E. Matijevic (Ed.), *Surface and Colloid Science*, vol. 7, John Wiley & Sons, NY, 1974.
- [45] R.W. O'Brien, Electro-acoustic effects in a dilute suspension of spherical particles, *J. Fluid Mech.* 190 (1988) 71–86.
- [46] R.W. O'Brien, Determination of Particle Size and Electric Charge, US Patent 5 059 909, Oct 22, 1991.
- [47] H. Ohshima, Dynamic electrophoretic mobility of spherical colloidal particles in concentrated suspensions, *J. Colloid Interface Sci.* 195 (1997) 137–148.

- [48] A.S. Dukhin, H. Ohshima, V.N. Shilov, P.J. Goetz, Electroacoustics for concentrated dispersions, *Langmuir* 15 (10) (1999) 3445–3451.
- [49] H. Ohshima, A.S. Dukhin, Colloid vibration potential in a concentrated suspension of spherical colloidal particles, *J. Colloid Interface Sci.* 212 (1999) 449–452.
- [50] A.S. Dukhin, V.N. Shilov, H. Ohshima, P.J. Goetz, Electroacoustics phenomena in concentrated dispersions, effect of the surface conductivity, *Langmuir*, submitted.
- [51] S.S. Dukhin, V.N. Shilov, *Dielectric Phenomena and the Double Layer in Disperse Systems and Polyelectrolytes*, John Wiley & Sons, NY, 1974.
- [52] L.L. Foldy, Propagation of sound through a liquid containing bubbles, OSRD Report No.6.1-sr1130-1378, 1944.
- [53] E.L. Carnstein, L.L. Foldy, Propagation of sound through a liquid containing bubbles, *J. Acoust. Soc. Am.* 19 (3) (1947) 481–499.
- [54] F.E. Fox, S.R. Curley, G.S. Larson, Phase velocity and absorption measurement in water containing air bubbles, *J. Acoust. Soc. Am.* 27 (3) (1957) 534–539.
- [55] S. Ljunggren, J.C. Eriksson, The lifetime of a colloid sized gas bubble in water and the cause of the hydrophobic attraction, *Colloids Surf.* 129/130 (1997) 151–155.
- [56] A.S. Dukhin, P.J. Goetz, Method and device for characterizing particle size distribution and zeta potential in concentrated system by means of acoustic and electroacoustic spectroscopy, patent USA, pending.
- [57] A.S. Dukhin, P.J. Goetz, Method and device for determining particle size distribution and zeta potential in concentrated dispersions, patent USA, pending.
- [58] A.J. Babchin, R.S. Chow, R.P. Sawatzky, Electrokinetic measurements by electroacoustic methods, *Adv. Colloid Interface Sci.* 30 (1989) 111.
- [59] R.P. Sawatzky, A.J. Babchin, Hydrodynamics of electrophoretic motion in an alternating electric field, *J. Fluid. Mech.* 246 (1993) 321–334.
- [60] Takeda Shin-ichi, P.J. Goetz, Dispersion/flocculated size characterization of alumina particles in highly concentrated slurries by ultrasound attenuation spectroscopy, *Colloids Surf.* 143, 35–39 (1998).
- [61] Takeda Shin-ichi, T. Chen, P. Somasundaran, Evaluation of particle size distribution for nanosized particles in highly concentrated suspensions by ultrasound attenuation spectroscopy, *Colloids Surf.* 1999.
- [62] Takeda Shin-ichi, Characterization of ceramic slurries by ultrasonic attenuation spectroscopy, in: V.A. Hackley, J. Texter (Eds.), *Ultrasonic and Dielectric Characterization Techniques for Suspended Particulates*, American Ceramic Society, Westerville, OH, 1998.
- [63] A.S. Dukhin, P.J. Goetz, Characterization of chemical polishing materials (monomodal and bimodal) by means of acoustic spectroscopy, *Colloids Surf.* 158 (1999) 343–354.
- [64] T.H. Wines, A.S. Dukhin, P. Somasundaran, Acoustic spectroscopy for characterizing heptane/water/AOT reverse microemulsion, *J. Colloid Interface Sci.* 216 (1999) 303–308.
- [65] V. Crupi, G. Maisano, D. Majolino, R. Ponterio, V. Villari, E. Caponetti, *J. Mol. Struct.* 383 (1996) 171.
- [66] B. Bedwell, E. Gulari, in: K.L. Mittal (Ed.), *Solution Behavior of Surfactants*, vol. 2, Plenum Press, New York, 1982.
- [67] E. Gulari, B. Bedwell, S. Alkhafaji, *J. Colloid Interface Sci.* 77 (1) (1980) 202.
- [68] M. Zulauf, H.F. Eicke, *J. Phys. Chem.* 83 (4) (1979) 480.
- [69] H.F. Eicke, in: I.D. Rob (Ed.), *Microemulsions*, Plenum Press, New York, 1982, p. 10.
- [70] J.D. Nicholson, J.V. Doherty, J.H.R. Clarke, in: I.D. Rob (Ed.), *Microemulsions*, Plenum Press, New York, 1982, p. 33.
- [71] H.F. Eicke, J. Rehak, *Helv. Chim. Acta* 59 (8) (1976) 2883.
- [72] P.D.I. Fletcher, B.H. Robinson, F. Bermejo-Barrera, D.G. Oakenfull, J.C. Dore, D.C. Steytler, in: I.D. Rob (Ed.), *Microemulsions*, Plenum Press, New York, 1982, p. 221.
- [73] P.C. Cabos, P. Delord, *J. Appl. Cryst.* 12 (1979) 502.

- [74] S. Radiman, L.E. Fountain, C. Toprakcioglu, A. de Valleria, P. Chieux, *Prog. Colloid Polym. Sci.* 81 (1990) 54.
- [75] J.P. Huruguen, T. Zemb, M.P. Pileni, *Prog. Colloid Polym. Sci.* 89 (1992) 39.
- [76] M.P. Pileni, T. Zemb, C. Petit, *Chem. Phys. Lett.* 118 (4) (1985) 414.
- [77] A.V. Kabanov, *Makromol. Chem. Macromol. Symp.* 44 (1991) 253.

Further reading

- [78] R.R. Irani, C.F. Callis, *Particle Size: Measurement Interpretation and Application*, John Wiley & Sons, NY-London, 1971.
- [79] E. Dickinson, D.J. McClements, M.J.W. Povey, Ultrasonic investigation of the particle size dependence of crystallization in *n*-hexadecane-in-water emulsions, *J. Colloid Interface Sci.* 142 (1) (1991) 103–110.